Physica Medica 38 (2017) 122–139

Contents lists available at ScienceDirect

Physica Medica

journal homepage: http://www.physicamedica.com

Review paper

Beyond imaging: The promise of radiomics

Michele Avanzo [a,*], Joseph Stancanello [b], Issam El Naqa [c]

[a] Division of Medical Physics, Centro di Riferimento Oncologico Aviano IRCCS, Aviano, PN, Italy
[b] Centro di Riferimento Oncologico Aviano IRCCS, Aviano, PN, Italy
[c] Department of Radiation Oncology, Physics Division, University of Michigan, Ann Arbor, MI USA

ARTICLE INFO

Article history:
Received 31 December 2016
Received in Revised form 31 March 2017
Accepted 30 May 2017
Available online 7 June 2017

Keywords:
Radiomics
Modelling
Response
Textural
Quantitative imaging
Segmentation
Image features

ABSTRACT

The domain of investigation of radiomics consists of large-scale radiological image analysis and association with biological or clinical endpoints. The purpose of the present study is to provide a recent update on the status of this rapidly emerging field by performing a systematic review of the literature on radiomics, with a primary focus on oncologic applications. The systematic literature search, performed in Pubmed using the keywords: "radiomics OR radiomic" provided 97 research papers. Based on the results of this search, we describe the methods used for building a model of prognostic value from quantitative analysis of patient images. Then, we provide an up-to-date overview of the results achieved in this field, and discuss the current challenges and future developments of radiomics for oncology.

Contents

* Corresponding author.
E-mail address: mavanzo@cro.it (M. Avanzo).

http://dx.doi.org/10.1016/j.ejmp.2017.05.071
1120-1797/

1. Historical background

With the term "feature" we mean a descriptor of an image (e.g. of tumor or normal tissue regions) such as parameters derived from image intensity, texture, shape, etc. Although, the notion of using imaging features for predicting actions traces its roots to the early days of computer vision in the 1960s, its systemic application in medicine of imaging quantitative analysis only started in the 1980s [1]. This application has been primarily focused on computer-aided detection or diagnosis (CAD) [2,3]. CAD uses a set of quantitative image features describing the geometrical structure, intensity distribution and texture of a region of interest (ROI) that are used by statistical or machine learning classifiers in order to identify abnormal tissues in a variety of organs including liver, prostate, colon, breast. The output of this analysis is used by radiologists as a second opinion in detecting lesions and making diagnostic decisions [1–5].

CAD is often categorized into two major groups, computer-aided detection (CADe) and computer-aided diagnosis (CADx), the first focusing on a detection, localization and segmentation of lesions in medical images, the second on diagnosis, for example, distinction between benign and malignant lesions [3,6]. In CADe for breast cancer, features of the breast mammogram are used for detection of masses, architectural distortions, and microcalcifications. These can be detected using basic image enhancement methods, descriptors of statistical distribution of intensity values, and decomposition of the image through wavelet transforms in order to investigate differences between areas and background [2]. CAD algorithms are composed of two stages, detection and classification of suspicious regions into cancer or normal tissue. In the first stage, texture features are extracted from ROIs, automatically or manually contoured. Because many features can be extracted, CAD systems frequently incorporate feature selection algorithms to select the features contributing the most to diagnostic accuracy [4]. In the second stage a binary decision tree classifier is trained to distinguish lesion from normal breast tissue [7]. In contrast to CAD application in diagnostic radiology, we will be focusing on the extension of these quantitative imaging techniques into therapeutic oncology for the purpose of predicting response to treatment.

1.1. Definition of radiomics

The application of this approach to biological markers and therapeutic endpoints only started in past decade, when the concept of personalized medicine arose following the increasing use of genomics. Some early examples include the investigation of correlations between specific hepatocellular carcinoma imaging phenotypes with doxorubicin drug response in 2007 [8], and, in 2009, between PET-based features and response to radiotherapy [9].

Since 2010, this field has been formalized with the term "radiomics" [10,11]. The term originates from the words "radio" which refers to radiology, the science of acquiring medical images through the use of radiation (e.g., X-rays, CT, MRI). The suffix "omics" was first used in the term genomics to indicate the mapping of human genome. Later, this was widely used in biology as in the study of RNA (transcriptomics), proteins (proteomics), and metabolites (metabolomics), to emphasize the holistic feature of the research encompassing the entire view of a system [12]. Because radiomics combines quantitative analysis of radiological images and machine learning methods, it has its roots in CAD, and is considered as a new application of established techniques [13]. Two aspects of radiomics, however, are novel: the number of image features involved, which in CAD is usually 8–20, whereas in radiomics it is increased to a few hundred or thousands. Second, the domain of investigation for radiomics consists of association of features extracted form large–scale radiological image analysis with biological or clinical endpoints, resulting in both prognostic and predictive models [14]. Radiomics is a general science which can be applied to many biomedical areas, but the focus of this review will be primarily on oncological applications and its role in advancing personalizing cancer treatment.

It is currently recognized that solid tumors do not consist of a homogeneous entity, but rather are composed of multiple clonal sub-populations of cancer cells, exhibiting considerable spatial and temporal variability that could potentially yield valuable information about tumor aggressiveness [15]. Quantitative image features, called also "radiomic features" could provide richer information about intensity, shape, size or volume, and texture of tumor phenotype that is distinct or complementary to that provided by clinical reports, laboratory test results, and genomic or proteomic assays. Tumor molecular biopsy-based assays, besides being invasive, provide limited tumor characterization as the extracted sample does not always represent the entire population of tumor cells. Radiomics circumvents this by assessing the comprehensive three-dimensional tumor bulk by means of imaging information [16].

Different imaging modalities (e.g., MRI, CT, PET, ultrasound) are used as the basis for extracting these features [17]. The complete set of imaging features obtained for a patient using the available images is called the "radiome" [18]. A collection of features which holds prognostic and or predictive value is often called "radiomic signature". The fundamental hypothesis of radiomics is that quantitative analysis of tumor through a large amount of radiomic features can provide valuable diagnostic, prognostic or predictive information [19,20]. For tumors, heterogeneity assessed through imaging could be the expression of genomic heterogeneity, which would indicate worse prognosis, as tumors with more genomic heterogeneity are more likely to develop a resistance to treatment and to metastasize [21]. The aim of radiomics is to explore and exploit these sources of information to develop diagnostic, predictive, or prognostic radiomic model (signatures) to support personalized clinical decisions and improve individualized treatment selection [14].

2. Purpose of the work

Radiomics is a rapidly evolving field, and the purpose of the present study is to provide an update on its status. For this purpose, a systematic review of the literature is performed, with a primary focus on oncologic applications. The results of the literature search are used to provide an overview of the techniques and the results obtained in radiomics studies. Then, the current challenges and future developments of radiomics are discussed. The present overview, however, covers only the recent advancements in this field and is far from being a comprehensive discussion of medical image analysis. For further information, we invite the readers to refer to textbooks and reviews cited in the following sections.

Table 1
Overview of methods and results from studies in which a radiomic model with prognostic value was built from imaging and outcome data of a dataset of more than 50 patients.

First Author, Ref. n°	N° of patients in training set (validation set)	Pathology	Endpoint	Image modality	N° features	Overview of features	Model building method	Most significant findings, Predictive power of model
Aerts [16]	1019	422 Lung1 (training), 225 Lung2, 136 H&N1, 95 H&N2	Survival, gene-expression	CT	440	First order, shape, texture, wavelet	Multivariate Cox proportional hazards regression	Radiomic signature (Statistics Energy, Shape Compactness, Grey Level Nonuniformity, wavelet Grey Level Non uniformity HLH) has CI on the Lung, first and second H&N dataset of 0.65, 0.69, 0.69
Coroller [28]	98 (84)	Lung adenocarcinoma	Distant metastasis	CT	635	Shape, statistics, GLCM, GLRLM GLSZM wavelet, Laplacian of Gaussian	Feature selection with mRMR, Cox regression	Radiomics signature built with: Wavelet HHL – Skewness, GLCM – Cluster shade and LoG 5 mm 2D – Skewness. CI = 0.61 of combined model on indipendent dataset
Coroller [55]	127	NSCLC	Pathological response to neoadjuvant chemoradiation assessed at time of surgery	CT	1603	Same as [28]	Features with an AUC above 0.60 and a p-value below 0.05 were considered predictive. Logistic regression	AUC for conventional, radiomics and combined models of 0.57, 0.65 and 0.65 for gross residual disease; 0.60, 0.61 and 0.68 for complete response
Emaminejad [142]	79	NSCLC	Recurrence	CT	35	GLRLM. GLCM,	CFS Subset Evaluator, Best-First heuristic feature search and selection method, Naïve Bayesian network based classifier	AUC = 0.84 radiomic and genomic markers
Fried [101]	91	NSCLC, III Stage	Local control, OS, distant metastases after CRT	CE-CT, 4-D CT	66	Absolute gradient, GLCM, NGTDM, Laplacian of Gaussian	Cox proportional hazards model with covariate selection	Classification rate 80%
Ghosh[143]	78	Renal cell carcinoma	(BAP1) gene alterations	CE_CT Multi-phase	572	Wavelet, Laws'filters, Laplacian of Gaussian, GLCM, global	Coefficient of variation (CV) criterion, Random forests	AUC = 0.55–0.71 according to CT phases of contrast
Gnep[78]	144	Prostate	Gleason score, biochemical recurrence after RT	T2-w and ADC MRI	147	Global, shape, GLCM Sobel, Kirsch filters	Random survival forests, LOOCV	T2 w and ADC features correlated with Gleason score and biochemical recurrence CI of combined model 0.9
Guo [76]	91	Breast cancer	Genetic expression		38 radiomic, 144 genomic	Size/shape/texture (GLCM), kinetic curve	Logistic regression with LASSO	AUC for stage, lymph node metastases, ER, PR, HER2, of 0.877, 0.693, 0.789, 0.689, 0.641 with radiomics only. No improvement after combining with genomics
Huang et al. 2016 [21]	282	NSCLC	Disease free survival after end of RT (DFS)	CE-CT	132	Global, GLCM, Laplacian of Gaussian	Feature selection with (LASSO) Cox regression Model	Radiomic signature based on kurtosis, uniformity, homogeneity on CE, uniformity on UE Radiomics nomogram CI = 0.72
Huang [90]	326 (200)	Colorectal cancer	Lymph node metastases	CT	150	Texture	Feature selection with LASSO, multivariable logistic regression	Nomogram including the 24 features radiomics signature, LN status, and carcinoembryonic antigen level (CI 0.778 in validation cohort)
Huynh 2016 [56]	113	Lung NSLC	Progression, distant metastases after SBRT	(CE-) CT	1605	Same as [28], Laplacian of Gaussian	Stable features selected from test–retest on RIDER dataset, PCA	3 conventional and 4 radiomic features prognostic for OS Median CI of radiomic models 0.67
Kickingereder [53]	119	GBM	PFS and OS	CE T1-DWI, FLAIR MRI	188	Global, shape, texture	Supervised principal component (SPC)	Stratification of patients for low- and high-risk for PFS p = 0.032 and OS p = 0.004 in validation set
Li [49]	84	Breast	Molecular subtype	T1w CE MRI	38	Size, shape, morphology, enhancement texture, kinetic curve, variance kinetics	Semi-parametric 'proper' binormal ROC model, LOOCV	AUC values of 0.89, 0.69, 0.65, and 0.67 For distinguishing between ER, PR, HER2, and triple negative statuses
Li [66]	93	Breast	Recurrence as given by multigene assay scores	T1-w, DCE MR	38	Size, shape, margin morphology, enhancement GLCM, kinetics	Logistic regression, LOOCV	AUC of 0.55–0.88 for different multigene assay risk of relapse
Liang [91]	286 (208)	Colorectal cancer	Pre-operative staging	CT	>133	Laplacian of Gaussian, global, GLCM	LASSO logistic regression model	Radiomic signature AUC of 0.792

Liu [99]	42 (11)	Nasopharyngeal	Response to chemo-RT	T1-, T2-, DWI MR	126	GLCM, GLGCM, Gabor, GLSZM	Fisher coefficient, mutual information for feature selection, k-nearest neighbors and artificial neural network for classifier	Models specificity: 0.667–1, precision: 0.857–1, F-score 0.643–0.889
Liu [60]	298	Lung adenocarcinoma	EGFR mutation	CT	219	Size/shape, global, GLRLM, GLCM, Laws texture, wavelet	Logistic regression	11 features were related to EGFR AUC of model 0.709
Nie[48]	48	Locally advanced rectal cancer	Pathological response	T1/T2, DWI-MRIDCE-MRI	103	GLCM, enhancement kinetics	Artificial neural network (ANN) with 4-fold validation technique	AUC of combined features 0.84 for complete response and 0.89 for gross residual disease
Ohri [43]	201	NSCLC	Overall Survival	PET	45	Global, GLCM, GLRLM, GLSZM NGTDM; SUV_{max}, MTD	LASSO	SumMean is an independent predictor of OS Patients grouped in three OS cathegories using MTV and Summean
Parmar [88]	101 (95)	Head and neck SCC	OS	18FFDG-PET-CT	440	Same as [16]	13 feature selection methods, 11 classifiers	AUC of classifiers 0.61–69
Parmar [27]	878	Lung and head and neck	Prognosis, histology, stage, Head and neck HPV status	CT	440	Same as [16]	Consensus clustering	Prognosis Lung CI = 0.60, Prognosis H&N CI = 0.68; Lung histology AUC = 0.56, Lung stage AUC = 0.61, H&N stage AUC = 0.77.
Vallieres [15]	52	Soft tissue sarcoma of extremities	Distant metastases	T1 T2 PET	41 texture, 9 non texture	Fusion, wavelet, SUV, shape, GLCM, GLRLM, GLSZM and NGTDM	Stepwise forward feature selection, logistic regression	Combination of four texture features extracted from FDG-PET/T1 and FDGPET/T2 FS scans gave AUC = 0.984
Wang [68]	84	Breast cancer	Triple-negative histology	(DCE) MRI	85	GLCM, clinical, size and shape, kinetics	Ranking and sequential forward floating search algorithm for feature selection, SVM	Models with features from tumor and surrounding parenchyma, AUCs 0.789–0.878
Wu [54]	198 (152)	NSCLC	Tumor histology	CT pre-treatment	440	First-order, shape, GLCM, GLRLM, wavelet (same as [16])	Many feature ranking methods and classifiers (including Relief, random Forests).	53 features associated with tumor histology Radiomic signature AUC = 0.72
Yang [52]	82	GBM	Molecular subtype, 12-months survival	T1, T2, FLAIR MRI	976	Fractal, histogram of oriented gradients, local binary patterns, GLRLM, GLCM	Random forest	AUC 0.72–0.82 for subtypes, 0.69 for 12 months survival
Yoon [25]	539	Lung adenocarcinomas	ALK/ROS1/RET chromosonal rearrangements that lead to gene fusions	CT and PET	51 radiomic, 4 clinical 6 qualitative	Global, texture	Features with a p value <0.1 for each category were selected, logistic regression.	Prediction model sensitivity 0.7344, specificity 0.7031
Ypsilantis[34]	107	Esophageal cancer	Response to neoadjuvant chemotherapy	PET	85 texture, 18 SUV based	GLCM, GLRLM, GLSZM, GLDM, Fractal-based, NGTDM, SUV	Convolution neural networks, logistic regression, random forest, and SVM	NGTDM coarseness is the most important feature Neural network model achieves an average 80.7% sensitivity and 81.6% specificity

2.1. Systematic review of literature

A literature search was performed, starting with a search performed in Pubmed using the following keywords: "radiomics OR radiomic". The search was completed by December 10, 2016. Studies in languages other than English, and studies only available in abstract form were excluded from this review except when they brought relevant novelty elsewhere unavailable (e.g. pathology not studied elsewhere). The review papers were included when relevant to introduce or discuss concepts of interest. The search provided 116 publications, of which 16 were reviews. Three studies [22–24] were discarded as not related to radiomics. The remaining 97 papers were included in the present report. A finer research was performed to include only studies in which a radiomic signature of prognostic value was developed from a dataset of at least 50 patients (see Table 1). When relevant, references within the searched papers were also considered.

3. The radiomics framework

The process of building a radiomic signature of prognostic/predictive value has four stages [14,20,25–28]: the first step involves image acquisition, followed by automated or manual segmentation of ROI. Then image features are extracted. Finally, a mathematical model is built and its value for prognosis or prediction of outcome of interest is assessed. A summary of the methods for each phase are presented below.

3.1. Acquisition of images

CT The most widely used imaging modality in radiomics studies is CT, which assesses tissue density, shape and texture of tumor and lymph-nodes [16,21,29]. One of the first studies on textural features identified texture measures correlation and difference entropy as the top features in discriminating between benign and malignant nodules in the lung [30]. CT has also the potential to measure size and/or change in size during and after therapy in order to early assess treatment response, as shown in Fig. 1. The administration of contrast for acquisition of contrast-enhanced CT (CE-CT) can improve the discrimination of necrotic tissue, which may exhibit reduced attenuation whereas vascularized tumor areas will appear brighter after contrast enhancement [31].

Texture features of NSCLC extracted from CT are related to tumor metabolism, PET tumor stage [32] and histopathology [31]. For some tumors, radiologic CT characteristics such as necrosis, calcifications, nodular tumor enhancement are related to mutations of genes, which are associated with advanced stage, advanced grade, and possibly worse cancer specific survival [33]. In *in vivo* preclinical models, radiomic features extracted from CT scan were able to identify early effects of changed gene expression, eventually combined with radiation treatment [19].

PET is used for detecting and staging cancer, most commonly with the radiotracer 18F-fluorodeoxyglucose (18F-FDG), a radiolabelled sugar (glucose analog) molecule [34] because the vast majority of malignant cancer phenotypes exhibit an increased glycolytic rate [35]. Other tracers include 18F-labeled 39-deoxy-39-fluorothymidine (18FFLT), the retention of which correlates with tumor proliferation [36], and [11C]Choline, based on the association of upregulation of choline kinase with cancer [37]. PET has been a hotbed for radiomics application to the functional nature of the images and their direct relationship to underlying tumor biology [38]. Tumor standardized uptake volume (SUV) and texture of PET characteristics are correlated with the development of metastatic disease and death in cervical cancer [39], and with survival [40] and chromosomal rearrangements that lead to gene fusions in lung cancer [25].

Texture analysis has been widespread in PET since the end of 2000s [41]. In a study on soft-tissue sarcoma, radiomic features were extracted from the fusion of FDG-PET and MRI volumes [15]. The change in PET uptake can be used to assess response to therapy [42]. A multi-institutional study identified that PET textural features are complementary to tumor volume in predicting overall survival (OS) in lung cancer, as shown in Fig. 2 [43].

MRI provides high-contrast structural and functional information to characterize soft tissue. One of the first radiogenomic studies based on MRI highlighted that enhancing areas in MRIs and CT scans overlapped with areas of neovascularity and cell proliferation as determined through biopsy [44]. Radiomic features have been used to discriminate prostate cancer from healthy tissue [45,46].

Dynamic contrast-enhanced (DCE) MRI characterizes the concentration of an injected gadolinium contrast agent over time [20,45]. and enables the visual differentiation of lesions from normal tissue owing to the increased vascularity and capillary permeability. By exploiting enhancement kinetics, the time course of the signal intensity within the lesion can be used in the interpretation of lesions to determine the likelihood of malignancy [47]. Texture feature of DCE-MRI separated response groups according to response (pathological-complete-response (pCR) or good response) after chemo-radiation for rectal cancer [48].

Radiomics features were able to distinguish status of expression of estrogen receptor (ER), progesterone receptor (PR), human epidermal growth factor 2 receptor (HER2), and triple negative (lack of expression of ER, PR, and HER2) for breast cancer from CE-MRI [49]. An example of different radiomic features extracted from CE-MRI of breast cancers with different ER status is shown in Fig. 3.

Diffusion-weighted imaging (DWI) MRI characterizes changes in the cellular architecture of the tissue based on local differences in movement of water protons [20,36]. DWI with Apparent Diffusion Coefficient (ADC) map [50] has been hypothesized to indicate cell death after therapy [51]. T2-weighted Fluid Attenuated Inversion Recovery (FLAIR) is a sequence, whose hyperintensity is

Table 2
Radiomic features extracted from CT scans of patients treated for lung cancer shown in Fig. 1. The features are: Radius_std, standard deviation of tumor radius, Gabor_Energy-dir135-w3 and Gabor_Energy-dir45-w9: energy calculated on the images after applying the Gabor filter built with orientations of 135/45° and wavelengths of 3/9 pixels. Shape_SI6 describes the local surface shape, and Shape_SI6 the saddle ridge shape. Laws_Energy-10 and 13: Energy calculated on the images processed by Laws filters number 10 and 13. Laws Energy 10 extracted from the pre-treatment scan was predictive for mutational status, as well as the difference in Gabor Energy and tumor volume between baseline and followup scan (adapted from [100]).

EGFR status	CT acquisition	Volume	Radius_Std	Shape_SI6	Gabor_Energy-dir135-w3	Gabor_Energy-dir45-w9	Laws_Energy-10	Laws_Energy-13
EGFR positive	Baseline (Fig. 1a)	7766.5	1.522	0.145	5337.9	419770.4	475.2	1369.6
	Followup (1-b)	7195.8	1.657	0.151	4043.5	327365.1	512.0	1352.9
	Change	−570.6	0.135	0.006	−1294.4	−92405.3	36.8	−16.6
Wild type	Baseline (Fig. 1c)	3502.4	1.422	0.173	11601.7	419578.9	367.7	353.9
	Followup (1-d)	4522.8	1.251	0.165	10605.5	361191.5	326.3	349.3
	Change	1020.4	−0.171	−0.009	−996.2	−58387.4	−41.5	−4.5

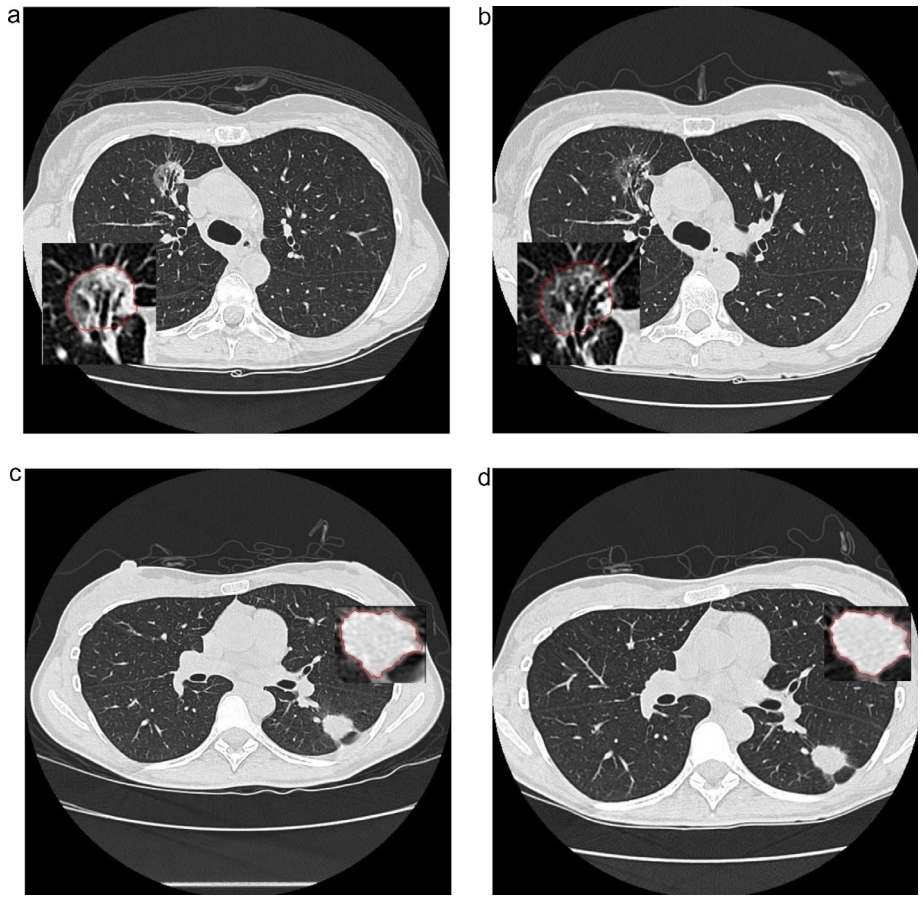

Fig. 1. CT images of a patient (1-a and 1-b) with EGFR mutation, and one (1-c and 1-d) with wild-type status. Images were acquired prior (1a and 1-c) and after (1-b and 1-d) administration of chemotherapy for lung cancer. Some radiomic features related to tumor phenotype and response to therapy extracted from these images, are shown in Table 2 (reproduced from [100] under Creative Common License).

generally interpreted as infiltrative tumor cells and vasogenic edema [51]. FLAIR radiomic features were associated with Glioblastoma Multiforme (GBM) molecular subtypes [52] and were identified to be the predictive for treatment outcomes in GBM [53].

3.2. Segmentation of region-of-interest

The calculation of radiomic features is typically applied to a specific ROI which needs to be segmented from the surrounding tissues, such as the gross tumor. In most radiomics studies, the tumor is manually delineated by an experienced radiologist or radiation oncologist [15,16,54–56]. However, a number of algorithms have been developed for automatic or semi-automatic segmentation. Region growing is a semiautomatic method often applied to the segmentation of masses in CAD in which, starting from a seed pixel chosen from the operator, neighboring pixels are iteratively added to the foreground region if they fulfill a similarity criterion [7]. In another semi-automatic approach, the user manually selects a ROI encompassing the lesion on a single slice and then the watershed method generates an initial three-dimensional surface of the lesion, subsequently refined by the active geometric contours [57]. Another semi-automatic algorithm delineates regions of consolidation within the lung, and is initiated by user's measurement of the tumor's longest axial diameter based on the Response Evaluation Criteria in Solid Tumors (RECIST 1.1) [58,59].

A CT-based semiautomatic method involving a multi-seed point segmentation routine (where the user places seeds identifying body, background, lungs and bones and the perceived center of the lesion) has been used for radiomics of lung tumor [60]. The method showed a high correlation of maximal diameters of the segmented tumor with that of the surgical specimen [61].

PET segmentation is affected by the high noise characteristics of the images. Lung tumor contour can be semi-automatically delineated in FDG-PET by a relative threshold method [62,63] or variational approaches, that attempt to exploit gradient differences between the foreground lesion and the background for the segmentation task, which may result in errors due to noise effects [64]. A commercially available software (MIM Software Inc.) includes a semiautomatic gradient-based delineation method used for segmentation of esophageal cancer [65].

Automatic segmentation of breast tumor in MRI has been used since more than 10 years in CAD with results comparable to those obtained with radiologist's delineation [66,67]. In a breast cancer radiomics study [68], the affected breast, tumor and its surrounding parenchyma were segmented semi-automatically on MRI datasets acquired before and at 1 and 2 min after contrast injection. Subsequently, the non-tumor breast tissue was then separated into fibroglandular parenchyma and adipose tissue semi-automatically on the pre-contrast images, using an adapted fuzzy c-means clustering technique [69] which assigns a membership to each voxel initiated with user-seeding and automatically determines the optimal threshold for parenchyma and adipose tissue separation. Extraction of radiomic features from hepatocellular carcinoma have been performed using core sampling, a method where samples were obtained by automatically tracing the maximal circle inscribed in the manual outlines [70].

Recently, a fully automatic segmentation tool for brain tumors (BraTumIA) and their compartments [71] have been proposed. Automatic prostate cancer segmentation was performed using

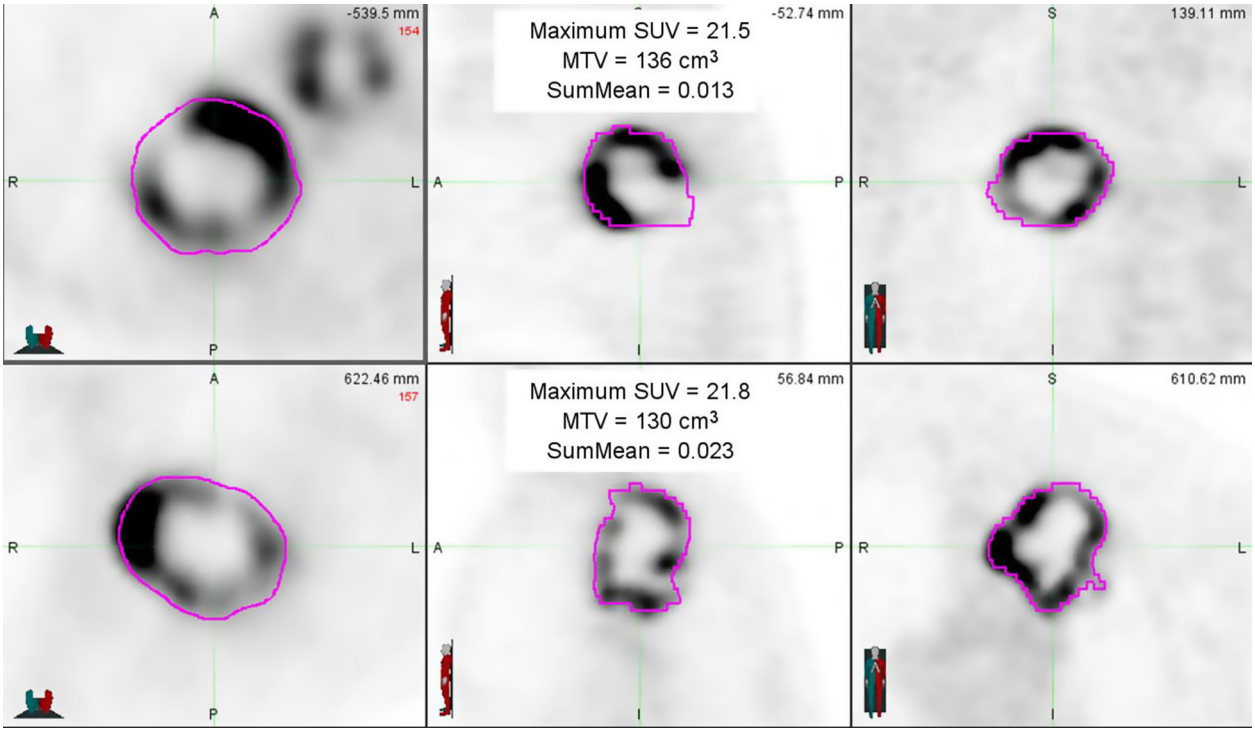

Fig. 2. PET images from two sample patients whose tumors had similar MTV and SUVmax and similar appearances, but had disparate SumMean values. Both tumors were scored as markedly heterogeneous based on visual examination. Survival time for the patient in the upper panel was 15.5 months, compared to 47.8 months for the patient in the lower panel (reproduced with permission from [43]).

multi-parametric MRI, which included T2-weighted, DWI, computed high-b DWI, and correlated diffusion imaging [45,46].

3.3. Extraction of radiomic features

In radiomics, large amounts of quantitative imaging features are extracted and analyzed. Examples of radiomic features extracted from images describing differences in tumor appearance are shown in Figs. 1–3. With the term "signature" we intend a collection of features which hold prognostic and/or predictive value, also known as Quantitative Imaging Biomarkers (QIB). Radiomic features are extracted after image preprocessing and filtering, as described in Appendix A1, which aims at reducing noise and enhancing characteristics of the image such as edges.

Comprehensive overviews of formulas for features are included in the supplementary materials of radiomics studies [28]. Kickingereder et al. [53] have provided a thorough review of formulas in their supplementary material, where the formulas of 188 features are shown. Radiomic features can be divided into: shape/size, first order histograms or global statistics, second order histograms or textural (see below). Some radiomic features are specific to an image acquisition method, e.g. SUV metrics in PET. Other recently introduced categories include fractal and fusion features applicable only to multimodal datasets. Software packages which perform radiomic features extraction and analysis are becoming available such as the "Imaging Biomarker Explorer" (IBEX) [72] which can also calculate radiomic models. CGITA [73] and Mazda [74] are open-sources software package for texture analysis which computes a number of features on a user selected VOI.

Size and shape features, such as volume, surface area, 2D and 3D maximal diameter, and effective diameter (diameter of a sphere with the same volume as the ROI), describe the size of the ROI. Surface to volume ratio, compactness, eccentricity, sphericity, of the tumor or of the ellipsoid that best fits the ROI, and standard deviation of tumor radius describe how much the tumor resembles a sphere. Solidity is the ratio of the number of voxels in the tumor region to the number of voxels in the smallest polyhedron containing the tumor region [9,15,16,55]. The margin morphologic appearance is described by margin sharpness, which is the mean of the image gradient at the lesion margin, and variance of margin sharpness [66].

First-order histogram or global statistics describe features related to the distribution of the intensities of voxels within the ROI, ignoring the spatial interactions between them, and can be calculated from histogram analysis, as mean, minimum, maximum, and standard deviation. The skewness and kurtosis measure the degree of histogram asymmetry and sharpness, respectively. The uniformity and entropy of the image histogram reflect inhomogeneity. These variables can be calculated in a n x n neighborhood of each voxel of the input image in order to map local changes in intensity distribution [14,32].

SUV-related features calculated from PET belong also to the group of global statistics: SUV_{max}, i.e. the maximum uptake in the ROI, SUVmean, i.e., the average uptake in the ROI, and SUV_{peak}, i.e., the average uptake in the neighborhood ($3 \times 3 \times 3$) of SUV_{max}. Other PET-related global features are metabolic tumor volume (MTV) and total lesion glycolysis (TLG) [62,63].

When considering the time course of signal intensity within the lesion after contrast injection, e.g. in CE imaging, it is possible to focus also on enhancement kinetics, that can be described by the average intensity in a ROI at each time point. Its peak value or "maximum uptake", the time frame index at which the maximum uptake occurs or "peak location", uptake rate (maximum uptake/-peak location), and washout rate can then be used as descriptors [75]. Enhancement-variance dynamics describes the time course of the spatial variance of the enhancement within the lesion, while enhancement-variance kinetics yields features such as variance increase rate and variance decrease rate [66,76].

Second order histogram or textural features, firstly introduced by Haralick et al. [77], describe the spatial distribution of voxel intensity levels. The term image texture refers to the perceived or measured spatial variation in the intensity levels, which can be visualized as a gray level scale [78]. The gray-level co-occurrence matrix (GLCM) is a matrix whose row and column numbers represent gray values, and the cells contain the number of times corresponding gray values are in a certain relationship (angle, distance) [77–79], as shown in Fig. 4. Features calculated on GLCM include entropy (second-order entropy, related to heterogeneity), energy (also defined as angular second moment, again describing the homogeneity of an image), contrast (which measures local variation), cluster shade (sensitive to heterogeneity), homogeneity, dissimilarity and correlation [80]. A 3D GLCM feature can be calculated as the mean of the feature values for each of the directions on which the GLCM is calculated [16]. GLCM can be calculated also for each voxel in an image within its $9 \times 9 \times 9$ neighborhood to reveal differences in regional heterogeneity [14].

Gray-level run is the length of consecutive voxels having the same intensity in a preset direction in the image, A gray level run-length matrix (GLRLM) [81] is a two-dimensional matrix in which each element (i,j) describes the number of times j a gray level i appears consecutively in the direction specified [34,54]. Short Run Emphasis, Long Run Emphasis, Short Run Low/High Gray Level Intensity, Long Run High/Low Gray Level Intensity, Run Length Non-uniformity, Run Percentage, Intensity Variability, Run Length Variability, High/Low Gray Level Run Emphasis are calculated from GLRLM [34].

Gray Level Size Zone Matrix (GLSZM) [82] is a matrix in which the element at row *r* and column *s* stores the number of zones (the connected voxels with the same gray level) with gray level *r* and size *s*. Therefore, a wide and flat matrix indicates that the ROI is homogeneous; a narrow matrix indicates heterogeneous ROI. Among the features calculated from GLSZM there are: Small/large Zone Emphasis, and low/high gray level zone emphasis, describing the distribution of small/large zones and zones with low/high gray levels [63].

In the neighborhood gray-tone difference matrix (NGTDM), the ith entry is a summation of the differences between all pixels with gray-tone i and the average value of their surrounding neighbors [15,34,83]. Radiomic features from NGTDM include coarseness, contrast, busyness, complexity, texture strength. Coarseness is high in images showing neighborhoods of fairly uniform voxel values; busyness, in contrast, is high in images with high spatial frequency of intensity changes [80,84].

Fusion features are related to multimodal image datasets which can be geometrically aligned by registration. Discrete Wavelet Transform (DWT) can then be applied to the registered datasets to combine the spatial and frequency characteristics of multimodality images. In the work of Vallieres [15] PET and MRI were fused into PET/MRI scans. The weight of MRI wavelet sub-bands in the FDG-PET/MRI fusion process and the presence or not of

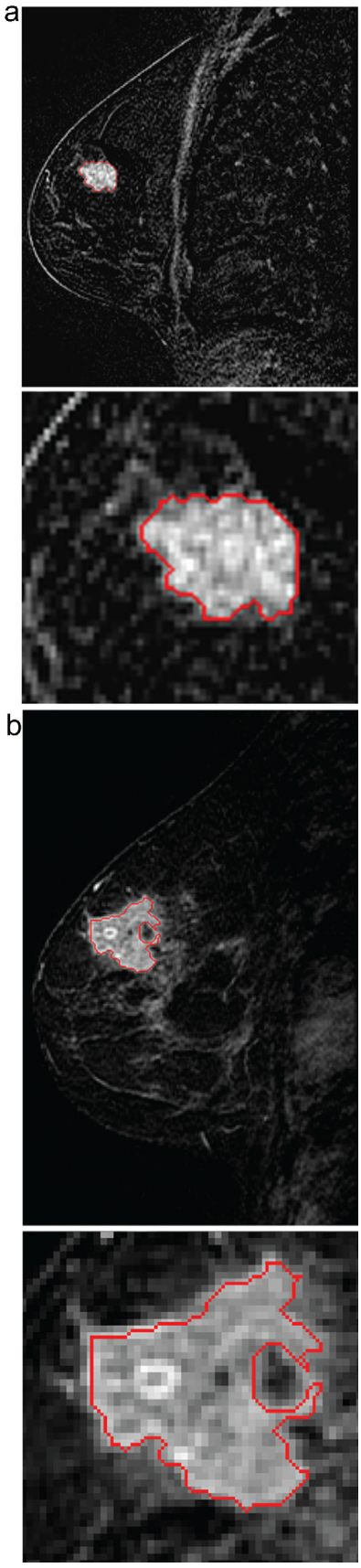

Fig. 3. Extraction of radiomic features from MRI images of breast cancer patients with different prognosis. In Fig 3a, sagittal MR images of a 75-year-old woman evaluated as having an ER-positive, PR-positive, HER2-negative, lymph node-negative, stage II invasive breast cancer with potentially good prognosis. The segmentation (red overlay) of the primary tumor is shown. The effective diameter, shape irregularity, entropy, and maximum correlation coefficient of this tumor are 16.8 mm, 0.438, 6.27, and 0.843. In Fig 3b, images of a 44-year-old woman evaluated as having an ER-negative, PR-negative, HER2-negative, lymph node–negative, stage II invasive breast cancer with poor prognosis. The effective diameter, shape irregularity, entropy, maximum correlation coefficient of this tumor are 21.7 mm, 0.592, 6.51, and 0.732, respectively (reproduced from [66] with written permission).

Test image	GLCM 0°	GLCM 90°	GLCM 135°
0 0 1 1	4 2 1 0	6 0 2 0	2 1 3 0
0 0 1 1	2 4 0 0	0 4 2 0	1 2 1 0
0 2 2 2	1 0 6 1	2 2 2 2	3 1 0 2
2 2 3 3	0 0 1 2	0 0 2 0	0 0 2 0

Fig. 4. Example of calculation of GLCM (adapted from Haralick [77]).

inversion of MRI intensity values were studied as radiomic features applicable only to fused images. This analysis showed that such fused features could be superior to using separate features extracted from individual images.

Fractal features Fractal analysis evaluates the self-similarity and roughness of a surface at different levels [52]. The complexity of these regions is quantified by the Hausdorff's fractal dimension (FD) [52], which refers to self-repeating textures of a pattern as one magnifies the feature. The FD of a 2D tumor area is defined as [52]:

$$D_0 = -\lim_{\varepsilon \to 0}(\log_\varepsilon N(\varepsilon)) = \lim_{\varepsilon \to 0}\frac{\log(N(\varepsilon))}{\log(\varepsilon^{-1})}$$

where N(ε) is the number of ε × ε squares needed to cover the 2D area. For digital images, the value of D_0 can be approximated by the box-count [85]. A fractal is defined as a set for which FD is strictly greater than the topological dimension. The FD of an object in an image ranges between 1 and 2 with higher values corresponding to increasing complexity [84]. Other fractal-related radiomic features are abundance and lacunarity [34,52,86,87].

3.4. Machine learning for building radiomics classifiers

The goal of radiomics is to develop a function or mathematical model to classify patients according to their predicted outcome by means of radiomic features. In the language of pattern recognition machine-learning, this task is equivalent to building a "classifier", which is an algorithm analyzing training data and inferring a hypothesis (the function), to predict the labels of unseen observations, e.g. patient outcome or tumor phenotype [88].

Feature selection: A large number of features can be extracted from each patient images, typically in the range of a few hundred to thousands (e.g. 219, 440, 1605, 6095 in [60,16,56,53] respectively), often largely exceeding the number of patients. Not all of the features, however, would be useful for a classifier to distinguish between patients of different classification, because some of them might be highly correlated with each other or redundant and some of them may not be strongly associated with the given classification task. By feature selection we intend an algorithm used to select "effective" features for a given task, i.e. those features who are relevant to explain a given output as a function of a group of features. The simplest feature selection method is to use a scoring criterion for the variables, based on the degree of stability or correlation of variables and remove those with worst ranking. Univariate methods for feature selection utilize variable ranking as the principal selection mechanism. Sometimes, it is defined a cutoff for "strong" univariate predictors [63]. The major disadvantage of these methods is that they do not consider the dependencies between different features that may lead to better prediction [13]. Multivariate methods investigate also the feature's association with the target/outcome variable [26].

In correlation-based feature elimination, highly correlated features are removed using a correlation matrix, so that, by eliminating those highly correlated features, we are left with "non-redundant" set of features. Column-wise average absolute correlation for each feature can be calculated from the matrix, and a threshold M is set for elimination, i.e., for each pair-wise correlation that exceeds M, features with higher column-wise average absolute correlation are removed [54,60].

The least absolute shrinkage and selection operator (LASSO) Cox regression model, is a shrinkage and variable selection method for regression models which maximizes a penalized log-likelihood function and is suitable for regression of high dimensional data [28,76].

One of the most used feature selection method is the minimum redundancy maximum relevance (mRMR), where the mutual information (MI) between a set of features and an outcome variable is calculated. Then, mRMR ranks the input features by maximizing the MI with respect to outcome and minimizing the average MI of higher ranked features [26,28,45,54,88].

One of the most recent, promising feature selection methods is RELIEF (RELevance In Estimating Features), where attributes are ranked using according to how well attributes distinguish among the instances that are near to each other. RELIEF can efficiently evaluate strongly inter-dependent features and showed higher prediction accuracy for radiomics as compared to other methods [54,63]. The RELIEF algorithms are able to detect context information among features and thus more accurately deal with situations where dependencies are present. However, RELIEF was also considered unable to detect redundant features which tend to have similar scores for evaluation. FAST (Feature Assessment by Sliding Thresholds), another feature ranking method, has the ability to tackle small sample size and imbalanced data problems [63].

Another method less commonly used in radiomics [20,34,89] is supervised principal component analysis (SPC), a transformation that converts the matrix of possibly correlated variables into a set of uncorrelated variables called principal components. The transformation is such that the greatest variance by any projection of the data would lie on the first coordinate (first principal component), the second greatest variance on the second coordinate (second PC), and so on [6]. As a result, a highly dimensional space can be reduced to a 2D or 3D space [20].

Other strategies to reduce features include choosing the most stable radiomic features based on test/retest analysis [56] and choosing the single feature with the highest performance for each category, e.g. statistics, shape, gray level, wavelet [16].

Model building and validation: Many methods have been used to build classifier models from radiomic features, many of which were previously developed for CAD [2]. In supervised classifiers, the training data consists of a set of examples, each example representing a pair of an input vector made of radiomic features of a patient of known outcome and the number describing his outcome. Supervised feature selection methods are prone to overfitting, an event in which, the model will better reflect noise in the image than the original data [13]. Among the most popular supervised classifiers in radiomics, possibly because of its simplicity, is logistic regression [15,25,27,34,48,55,66,76,78,90–92].

Random forest [27,34,45,53,54,78] is based on decision trees, a popular concept in machine learning especially in the field of

medicine, because their representation of hypotheses as sequential "if-then" resembles human reasoning [6]. In random forest methods a group of decision trees is trained, and the algorithm introduces two levels of randomization: first, it randomizes training samples by resampling with replacements (bootstrapping); second, at each branching step it chooses an attribute to split among a randomly selected subset of attributes. After a bag of trees is trained, prediction is made for all the individual trees and the most frequent class selected by the trees is taken as a final result [52].

SVM is a discriminative supervised machine learning technique previously used for CAD [2], which uses a boundary to separate data points into two categories, such as responders or not responders, that yielded high discriminative power in micro-calcifications detection in CAD [2] and frequently used in radiomics [27,34,45,58,63,68]. The boundary can be a complex hyperplane that maximize the margin between the two classes in a non-linear feature space. SVM also tolerates some points on the wrong side of the boundary, thus improving model robustness and generalization [93].

Artificial neural networks (ANNs), one of the classical machine learning methods [7], has been also used in radiomics for supervised classification [34,48,54]. A Convolutional Neural Network (CNN) is a special feed-forward neural network for learning a hierarchical representation of imaging data, operating directly on raw images, whereas other classifiers need prior extraction of relevant texture features from images. By attempting to automatically extract highly expressive imaging features, CNN removes the dependency on image preprocessing and choice of features to analyze. This method outperformed other predictive models for identification of triple negative breast cancer from MRI features [34].

Unsupervised classifiers are different from supervised classification methods, which incorporate a priori variables such as therapy response or survival information and do not need any training data. The goal of unsupervised classifiers is to identify a cancer subtype in the database of known patients with similar characteristics to the unknown cancer in terms of features [13,94]. The patients are grouped based on a distance metric. More recently one of the unsupervised machine learning methods, consensus clustering, was used to reduce a high dimensional feature space into fewer non-redundant feature clusters. The algorithm first performs subsampling of samples, and, for varying cluster numbers, calculates the consensus, defined as the proportion that two samples are placed in the same cluster out of the total number of times they appear in the same subsamples. For example consensus clustering could identify, in a feature space of 440 features, thirteen (size: 8 to 93 features per cluster) non-redundant feature clusters [27].

To quantify the discrimination performance, the AUC or the Harrell concordance index (CI) is used, which represents the probability that, among two randomly drawn samples, the sample with the higher risk value has also the higher chance of experiencing an event [28].

The most used technique for internal validation is the "leave-one out" cross-validation (LOOCV) procedure, also known as the "jackknife", where all the data are used for training/fitting except for one data point left out for testing, and this is repeated in each LOOCV iteration, so that each data point is left out exactly once [55,58,63]. Another method, the bootstrap, consists of generating a large number of bootstrap samples from the original data. A bootstrap dataset is a series of data (features, outcome), each from a patient chosen randomly from the cohort of patients and the model building is repeated for each bootstrap sample [16,90,95]. Both methods provide a distribution of values for model parameters and of the model evaluation index, AUC or CI, so that uncertainty can be evaluated. A more advanced bootstrapping method that combines characteristics from both LOOCV and standard bootstrap is the 0.632+ method [15,63].

4. Representative results of radiomics application in oncology

4.1. Overview of oncologic results from radiomic studies

Radiomics models have been built with power to predict tumor characteristics as histology [54], genetic footprint [25,60,96], as well as response to therapy in terms of pathological response from primary tumor [48,55] and lymph nodes [97], response to chemotherapy [98] or chemoradiotherapy [99], recurrence [66,78], occurrence of lymph nodes [90] or distant metastases (DM) [15,28,56], and survival [21,88], for a variety of pathologies. In this section, we will review some of the results obtained with radiomics according to the type of cancer.

Lung: Lung NSCLC is the tumor which has been most extensively studied and characterized through radiomics. The histological subtype, adenocarcinoma or squamous cell carcinoma, can be predicted with models trained on features extracted from pretreatment CT images. Using Relief feature selection method and the Naïve Bayes's classifier, a probabilistic classifier based on Baye's rule, a model was trained on a set of 440 3D radiomic features describing intensity, shape, and heterogeneity of the segmented tumor. A 5 variable model, mostly based on wavelet transforms, showed the highest AUC of 0.72 for tumor histology [54]. Radiomic features of NSCLC extracted from CT are related to tumor metabolism, PET tumor stage [32] and histopathology [31]. The identification of patients with presence of mutations of epidermal growth factor receptor (EGFR) in NSCLC is of great interest as they may respond to EGFR-targeted drugs and molecular methods used to detect EGFR mutations are expensive. Radiomic feature Laws-Energy on the pretreatment CT scan was significantly predictive for EGFR-mutation status[100]. A radiomic model for identification of EGFR mutant status from tumor segmented semiautomatically on CT using seed-based region growing method was developed through multiple logistic regression and pairwise selection with moderate predictive power (AUC, 0.647; 95% CI, 0.576–0.701). The model improved the AUC to 0.709 by including also clinical variables [60]. Radiomics can identify responders to treatment with gefitinib, a EGFR tyrosine kinase inhibitor, from the change in features between the CT acquisitions before and after three weeks of therapy (Fig. 1). The change in features between the two scans was strongly predictive (significant feature AUC-range = 0.74–0.91) [100].

A model for prediction of the appearance of chromosomal rearrangements that lead to gene fusions ALK, ROS1 and RET including clinical and radiomic variables extracted from PET and CT reached sensitivity and specificity of 0.73 and 0.7. Gene fusion have been become of clinical interest as fusion-positive patients may benefit by targeted drugs [25].

Including radiomic features together with conventional prognostic factors improves NSCLC patient risk stratification [101]. Multivariate models based on conventional, radiomics and combined features were created for predicting pathological response to neoadjuvant chemoradiation assessed at time of surgery [55]. The median AUC values from the cross validation were 0.57, 0.65 and 0.65 for gross residual disease and 0.60, 0.61 and 0.68 for pathologic complete response, for conventional, radiomics and combined models respectively.

In a radiomics study focused on the prediction of disease free-survival from CE and plain CT, a radiomic signature was based on kurtosis, uniformity and homogeneity from CE-CT, and uniformity from plain CT. The model was incorporated in a nomogram which outperformed (CI of 0.72) tumor staging for individualized disease-fee survival prediction [90].

A set of 1605 radiomic features was mined to describe the outcome of NSCLC patients after Stereotactic Body Radiation Therapy.

Five statistics and textural features were prognostic of local recurrence, three for lobar recurrence, and seven for overall survival. One feature, Wavelet LLH range, measuring the range of voxel intensity values in the wavelet-filtered image and related to tumor heterogeneity, was prognostic for developing DM. A radiomic signature composed of the top three features was trained for DM resulting in a CI of 0.67 [56].

A radiomic signature was developed to predicted DM after locally advanced adenocarcinoma [28]. Four features were prognostic for both DM and survival and were based on Laplacian of Gaussian (LoG) filter (CI > 0.60 with CI = 0.61 in an independent validation dataset). The radiomic signature consisting of Wavelet HHL–Skewness, Gray-Level Co-occurrence Matrix–Cluster shade, and LoG 5 mm 2D–Skewness, combined with clinical data, reached a CI of 0.6 for DM in the validation dataset.

Aerts et al. [16] built a radiomic signature consisting of a combination of four features, 'Statistics Energy' describing the overall density of the tumor, 'Shape Compactness' quantifying how compact the tumor shape is, 'Gray Level Nonuniformity' a measure for heterogeneity and wavelet 'Gray Level Nonuniformity HLH', also describing intra-tumor heterogeneity after decomposing the image in mid-frequencies. The signature was obtained by selecting the most stable features using the RIDER dataset, and then trained on a set of 422 lung cancer patients for the prediction of survival. The signature, assessed on an independent lung dataset, was predictive for survival (CI = 0.65), and was successfully tested on cohorts of different cancer types (lung, head and neck cancer) thus demonstrating the translational capability of radiomics in different cancers. In the same study, gene expression of 89 patients from a lung cancer cohort was measured for 21,766 genes, and revealed significant associations between the radiomic features and gene-expression patterns.

Ohri el al [43], has recently published a radiomics model from a multi-center data of 201 patients. Using the LASSO procedure they identified 1 textural feature calculated from GLCM, SumMean [77], as an independent predictor of overall survival that complement volume (MTV) in decision tree. The optimal cutpoint for MTV was found to 93.3 cm^3, and the optimal SumMean cutpoint for tumors above 93.3 cm^3 in the decision tree was 0.018.

Breast: A radiogenomic study demonstrated the associations of radiomic phenotypes such as tumor size, shape, morphology, enhancement textures, kinetic curve assessments, and enhancement-variance kinetics with breast cancer genomic features as miRNA expressions, protein expressions, gene somatic mutations, and transcriptional activities. In particular, the radiomic features had associations with transcriptional activities of pathways and miRNA expressions. Specifically, transcriptional activity of two signaling pathway, the JAK-STAT and TGF-beta, were associated with greater size and irregular shape, respectively. The pathway JAK-STAT had also associations with maximum enhancement and enhancement at first post-contrast time point, which implies different blood flow dynamics. The expressions of miRNAs were associated with tumor size and enhancement texture [96].

Classifier models based on radiomics were trained on MRIs of biopsy proven breast cancers from National Cancer Institute's multi-institutional Cancer Genome Atlas (TCGA) and Cancer Imaging Archive to predict immunohistochemistry molecular classification and reached AUCs of 0.89, 0.69, 0.65, and 0.67 in the tasks of distinguishing status of expression of ER, PR, HER, and triple negative, respectively [49]. Radiomic and genomic profiles were combined using data from the same database, with the aim of improving the predictive models for clinical phenotypes. The prediction performances by genomics alone, radiomics alone, and combined features showed statistically significant correlations with clinical outcomes; however, improvement on the prediction performance by combining genomics and radiomics data was statistically significant [76].

The differentiation of breast cancer subtype with DCE-MRI can be improved by including features of the parenchyma tissue surrounding the tumor. In particular, features 'Variance of parenchyma signal enhancement ratio', 'homogeneity of parenchyma percent enhancement', and 'cluster shade of parenchyma percent enhancement' proved to be effective discriminators of triple negative, ER+, and Luminal B types of cancer. By using both parenchyma and tumor features such as the AUC for predicting triple-negative breast cancer improved from 0.789 to 0.883. [68].

The risk of recurrence as predicted from multigene assays was investigated using computer-extracted tumor phenotypes of size, shape, margin morphology, enhancement texture, and kinetic extracted from MRI. Radiomic classifiers developed using logistic regression and validated with LOOCV were predictive for the risk of recurrence of breast cancer as predicted with three research-based multigene assays, with AUC values of 0.55–0.88 [66].

Radiomics has shown the potential to predict response to neoadjuvant chemotherapy. In analysis of DCE-MRI-based radiomic features, texture features based on GLCM on precontrast and 1–5 min postcontrast data were extracted and showed significant differences between responders and partial responders [98].

Prostate: Radiomic features, derived primarily from T2-w and ADC MRI scanning, correlate with Gleason score, which is probably the most powerful prognostic factor for prostate cancer, and are associated with biochemical recurrence following prostate radiotherapy. MRI scanning was performed using 3.0 T scanners. Features included first-order statistics, GLCM, and geometrical measurements computed in T2-w and ADC MRI. A random forest approach using five selected features: tumor volume, T2-w difference variance mean, T2-w contrast mean, maximal tumor area, and ADC median, demonstrated a CI of 0.90 for biochemical recurrence after radiotherapy [78].

GBM: The extraction of radiomic features from MR of GBM was able to predict immunohistochemically identified protein expression patterns [102]. A radiomic prediction model was designed for prediction of response to antiangiogenic therapy by stratification of patients according to progression-free and overall survival [89].

A radiomics analysis focused on a characterization of GBM diversity, using various diversity indices to quantify habitat diversity of the tumor. A classifier was then developed from these features to predict EGFR-driven tumors and 12-month overall survival. The model reached AUC of 0.85 and 0.74 for the two endpoints [103].

In another study [52] radiomic classifiers based on texture features calculated from postcontrast T1 and T2 weighted FLAIR were derived using random forest classifier for the identification of molecular subtype (classical, mesenchymal, neural, proneural) and prediction of survival at 12 months. Radiomic features included fractal, GLRLM, GLCM, local binary patterns (LBPs), and histogram of oriented gradients (HOGs). Model's AUC were 0.7–0.82 for molecular subtypes and 0.69 for 12-month survival status.

An 11-feature radiomic signature including first-order, volume, shape, and texture features from the multiparametric (unenhanced, CE-T1-weighted and FLAIR imaging sequences) MRI was identified allowing stratification of patients with newly diagnosed GBM into low- or high-risk group for PFS and OS. Imaging features such as standard deviation of energy and gray level run emphasis were significantly correlated with patient prognosis. The performance of the models identified using SPC analysis (CI of 0.654, 0.611 for OS and PFS) was higher compared with that of the radiologic (Gaussian normalized relative cerebral blood volume and apparent diffusion coefficient) and clinical (age and Karnofsky

performance score) risk models. The predictive power was further improved when combining radiomic with clinical data (CI, 0.696; 0.637 for overall survival and progression free survival) [53].

Most of GBM recurrences occur in the peritumoral brain zone. A preliminary study has shown that MRI derived radiomic features related to heterogeneity and texture extracted from the peritumoral brain zone, were predictive of survival [104].

Renal cell carcinoma (RCC): Treatment-related changes *in vivo* after early antiangiogenic therapy (sunitinib) for RCC were assessed using radiomic features obtained from FLT-PET/MRI in a feasibility study [36] where a map of integrated changes from PET/MRI radiomic features was created on two patients.

Head and neck: The radiomic signature developed on lung cancer cohort in the aforementioned study by Aerts et al. [16] was tested for prediction of survival on two cohort of squamous cell head and neck cancer. The model had a prognostic value with CI of 0.69 in both datasets.

Nasopharyngeal carcinoma is a relatively radio- and chemosensitive type of head and neck cancer. A total of 126 radiomic features were extracted using GLCM, GLGCM, Gabor transform, and GLSZM from contrast-enhanced 3.0T MRI using T1-w, T2-w, and DWI sequences to predict the therapeutic response of nasopharyngeal carcinoma (NPC) to chemoradiotherapy [99]. High sensitivity and specificity were obtained from all imaging modalities (T1: 0.952/0.939, T2: 0.904/0.905, DWI: 0.881/0.929) showing the potential for identification of responders.

Soft tissue sarcoma: Vallieres et al. used texture-based model for the early evaluation of lung metastasis risk in soft-tissue sarcomas [15] from pre-treatment FDG-PET and MRI scans comprising T1-weighted and T2-weighted fat-suppression sequences (T2FS). Nine non-texture features (SUV metrics and shape features) and forty-one texture features were extracted from the tumor region of separate (FDG-PET, T1 and T2FS) and fused (FDG-PET/T1 and FDG-PET/T2FS) scans. Volume fusion of the FDG-PET and MRI scans was implemented using the wavelet transform. A combination of four texture features extracted from FDG-PET/T1 and FDGPET/T2FS scans reached an AUC of 0.984.

Rectal/colorectal: A radiomic signature for preoperative prediction of lymph node metastases for colorectal cancer [90] consisting of 24 features, was extracted from an extensive series of patients and included in a nomogram with CT-reported LN status, and carcinoembryonic antigen level that showed CI 0.778 in validation cohort. In another study, preoperative identification of tumor stage with a 16 features radiomics signature achieved an AUC of 0.794 [91]. Pathologic response after preoperative chemoradiotherapy for locally advanced rectal cancer was studied in multiparametric MRI. A radiomic signature built from the best selected predictors as mean-ADC from DWI and GLCM_AutoCorrelation from DCE-MRI, could improve the AUC to 0.84 [48].

Other tumors: Radiomic CT features have shown the potential to predict intraductal papillary mucinous neoplasms, which are pancreatic cancer precursors incidentally discovered by cross-sectional imaging [105]. Accurate discrimination between responders and non-responders to chemotherapy after Non-Hodgkin lymphoma have been achieved using textural features from MRI [106].

4.2. Non-oncological applications

The radiomics approach of mining variables for prognosis could be applied to a number of other non-oncological fields. The change in texture feature values between pre- and post-radiotherapy CT scans can be used to characterize radiation-induced damage in the lung [107]. Neurology is a field where, for many applications, imaging features have been shown to be related to a clinical endpoint of interest. Possible neurological applications include the diagnosis, staging and prognosis of Alzheimer [108] and Parkinson's disease [109], as well as multiple sclerosis [110].

Vascular medicine could be another frontier for radiomics. Texture analysis of computed tomographic angiography was successfully used for the prediction of endovascular leak after endovascular prostheses [111]. CT image heterogeneity and PET SUV was correlated with expansion of abdominal aortic aneurysm [112].

5. The promise and challenges of radiomics

Radiomics is still in its infancy and great care is expected to realize all the promises so far envisioned. We will try to analyze its limitations, the possible paths for improvement on each step in the workflow, and discuss the possibilities for evolution in research and clinics.

5.1. Reproducibility

Repeatability is a measure of precision under identical or near-identical conditions and acquisition parameters [41], and is evaluated by "test-retest" analysis, a comparison of the results from images acquired within a short time on the same patient. A study on a dataset consisting of 31 sets of test-retest CT scans that were acquired approximately 15 min apart showed that the majority of the radiomic features are repeatable (concordance index >0.9) when acquired under the same imaging settings and semiautomatic segmentation. The dataset is now publicly accessible through The Reference Image Database to Evaluate Therapy Response (RIDER) [113].

Reproducibility or robustness, in contrast, is measured when measuring system or parameters differ. The major sources for variability of radiomic features are the imaging scanners, the parameters of acquisition and reconstruction of the image, and delineation of ROI.

For CT, inter-scanner variability of image features was investigated by comparing radiomic features extracted from phantom images acquired for 17 different CT. Inter-scanner variability produced differences in extracted features that are comparable to the variability found in a series of patients acquired in the same scanner [114]. The variability of radiomic features due to methods of reconstruction was studied a series of 42 CT images of pulmonary tumors, which were reconstructed with filtered back projection and a commercially available iterative reconstruction algorithm. The variability due to the reconstruction algorithms was significantly higher than inter-reader variability due to manual ROI segmentation for entropy, homogeneity, and GLCM based features [115]. Some features such as effective diameter, sphericity, entropy, and GLCM entropy were identified as robust to inter-reconstruction algorithm variability (coefficient of variation 5%) [115]. Smoothing of the image and reducing the slice thicknesses down to 1.25–2.5 mm can improve reproducibility of CT-extracted features [113,116,117]. CT also allows for 4-dimensional acquisition (4D-CT). On multi-modality CT scans, the greatest reproducibility was found on features generated from expiratory phase, followed by average intensity projection CT, and CE-CT [101].

In PET imaging, textural features are sensitive to different acquisition modes [118,119], reconstruction algorithms, and their user-defined parameters such as the number of iterations, the post-filtering level, input data noise, matrix size, and discretization bin size [37,120,121]. The stability of radiomic features extracted from FDG-PET/CT was studied when changing the delineation and reconstruction methods [87]. It was shown that, even if the majority of radiomic features were highly stable (interclass

correlation coefficient ≥0.90), twenty-five features were more sensitive to a change in delineation than in reconstruction method. In a study on a wide range of radiomic features in [18F]FDG and [11C]choline PET images of nasopharyngeal carcinoma, discretization (resampling the entire range of gray-scale values into a smaller number of groups or bins) had larger effects on feature variability than segmentation [37]. In presence of significant respiratory tumor motion as in the case of lung cancer, conventional PET images are influenced by motion as, because of their relatively long acquisition times, the counts measured are averaged over multiple breathing cycles. Respiratory-gated PET accounts for respiratory motion and textural features from gated PET have been found robust [62,122].

Radiomic features extracted from MRI images depend on the field of view, field strength and slice thickness. Results of the DCE MRI depend on the contrast agent dose, method of administration, and the pulse sequence used. The radiomic features extracted from DW-MRI depend on acquisition parameters and conditions as k-space trajectory, gradient strengths and b-values. The repeatability of MR-based radiomic features has not been investigated [123].

Segmentation represents one of the most critical steps in the radiomics workflow, because many extracted features may depend on the segmented region, and tumors may have indistinct or complex margins: this may potentially lead to inconsistency and lack of reproducibility of results. Manual delineation by an expert radiologist is considered the "gold standard", though it is prone to high inter-observer variability and represents a time-consuming task [17,20]. It was shown that the semiautomatic segmentation algorithm implemented in the 3D-Slicer open source platform, produce contours of lung tumor on CT which were more reproducible than manually drawn regions [61] and yield radiomic features with significantly higher reproducibility compared to those extracted from the manual segmentations [124]. Recently available fully automatic segmentation tools for brain cancer from MRI are as accurate as manual segmentation by medical experts [70].

The studies on the comparisons of the performance of many classifier and feature selection methods indicate that the choice of classification method is the most dominant source of models' predictive performance variability [26]. Fourteen feature selection algorithms were compared on a set of 464 lung cancer patients considering 440 radiomic variables [27]. The feature selection method based on the Wilcoxon signed-rank (WLCX) test had the highest prognostic performance with high stability against data perturbation. Interestingly, WLCX is a simple univariate method based on ranks, which does not take into account the redundancy of selected features during feature ranking. Wu et al. [54] compared the performance of 24 feature selection methods for radiomic signature building for lung cancer histology and showed that RELIEF with its variants were the best performing methods.

5.2. Sample size and statistical power

Many radiomics studies involve small numbers of subjects with respect to the number of radiomics features investigated [125], thereby raising the challenge of p-omics versus pan-omics as encountered in big data studies. Given the large number of imaging features extracted in radiomics studies, a small dataset reduces its power and increases the risk of overfitting the data.

Most radiomics studies do not report sufficient validations in independent cohorts, thereby limiting generalizability to additional patient populations, imaging by different scanner types, etc. At present, only one group performed external validation of their radiomics model [120]. Image data sharing across sites can be a solution to build large data sets for radiomics [14,20] and could serve as high-quality datasets to be used for external validation [126].Various online repositories of imaging datasets are already as the The Cancer Imaging Archive (TCIA) hosted by the National Cancer Institute [127], and the Lung Image Database Consortium, the Reference Image Database to Evaluate Response to therapy in lung cancer.

5.3. Standardization and benchmarking

Frequently, the images used in many radiomics studies are acquired from multiple institutions with various acquisition protocols [127] or with scanners from different vendors [4,60,78]. We believe that standardized acquisition and reconstruction protocol will be needed to smooth out input data variability, especially in view of multicenter studies that are expected to create the most robust models. Recommendations should be drafted regarding every step of the radiomics framework in order to achieve standardization and increase quality of radiomics studies. These should also cover: the discretization method and the bin size to be preferred [87], the preferred segmentation method (manual, semiautomatic or automatic), standard definitions of various radiomic features [41], and indications on which features are most stable [128]. For example, the GLCM feature 'Correlation' was found to be robust, regardless of the discretization method used [129]. The more reliable and efficient machine learning algorithms should also be indicated in order to identify stable and reproducible features in the high dimensional feature space created by radiomics [13].

There is need for benchmarks with the use of test objects with known physical properties values of radiomics features. Both digital [130] and physical [114] phantoms have been proposed with known features, the latter of which could be used for an 'end to end' test, for testing the entire radiomics chain from image acquisition to determination of prognostic output. The mathematical steps, as feature extraction and calculation could be tested using open-source verified formulae and codes. The publicly available cohorts of patients with image and clinical data should be used by research groups for benchmarking of a radiomics workflow. Finally, standards for publishing methods, results, and their uncertainty should be recommended, as well as ways to improve the peer review e.g. insist on at least one "statistical reviewer" with knowledge of machine-learning methodologies [41].

5.4. Limitations and pitfalls

The main criticisms to radiomics is that the link between the imaged properties of tumors and tumor biology is not straightforward. Most radiomics studies show statistical correlation between radiomic features and genetic footprint or prognosis, but correlation does not imply causation [125]. Establishing this link is necessary for tailoring the treatment to the individual patient based on the imaged properties of tumors [131]. A step forward was the preclinical investigation of Panth et al. [19], where a genetic tumor model was employed in which tumor microenvironmental characteristics like hypoxia change upon doxycycline administration. It was observed experimentally that a genetic change results in significantly different radiomics features, although these features were not consistent across the different imaging time points.

5.5. Future directions

The critical mass will be gathered especially in those pathologies considered *orphan* in that they are rare or not widely treated. We also believe that an effort will be need also from imaging device providers: for example, the current use of weighted images in MR prevents the development of MR based radiomics, while the possibility of having *quantitative* images (e.g., T1 and T2 maps) would significantly enable the use of MR in this field.

The advantage of using a radiomics approach relies also the possibility of extending the number of features potentially holding prognostic/predictive values without a significant burden: the radiomics platform will be able to automatically select the features and analyze the possible correlation. Therefore, we envision an extension of other features from advanced mathematical analytical tools, as already happened with fractal features. Most radiomics studies currently focus on single modalities, however, there is richer information in hybrid imaging that could be combined to develop a more complete picture of the tumor. Other 3D information, as dose distribution delivered in radiotherapy calculated on pre-treatment CT, could be integrated in the radiomics analysis. In addition, imaging information could be combined with other –omics data to create pan-Omics type models for detecting tumors boundaries, modeling response, and deciphering the underlying molecular biology [132].

Machine learning and the produced prediction models in radiomics have been so far dominated by "shallow" approaches, such as SVM. However, we already see a migration towards other machine learning tools such as deep learning and other advanced neural network approaches. In deep learning, multi-stack layers of modules with non-linear output perform the task of learning the representations of data with multiple levels of abstraction. Each non-linear model transforms the representation at one level. For example, the first level may represent edges in an image oriented in a particular direction, the second may detect motifs in the observed edges, the third could recognize objects from ensembles of motifs [133]. Patch-/pixel-based machine learning (PML) methods use pixel/voxel values in images directly instead of features calculated from segmented objects as in other approaches [134]. Thus PML removes the need for segmentation, one of the major sources of variability of radiomic features.

In the research area, radiomics is expected to spread where new signatures could be identified by means of data mining and correlation with endpoints. It means that, though currently many efforts are limited to oncology and cardiovascular diseases, all theragnostic approaches will be revised in view of radiomics, e.g., neurodegenerative and *orphan* pathologies. A particular role for radiomics as research tool will be in the drug development. The possibility of quickly assessing if the drug has reached the target and if it has produced the expected effect by means of non-invasive imaging will speed up the development of many, innovative personalized drugs, hopefully decreasing their development costs and, in turn, the burden for healthcare systems.

Radiomics is expected to increasingly affect the clinical practice, optimizing the end-to-end diagnosis-treatment-follow-up chain. It has been shown in a single-center trial that prediction of side effects made with statistical models can outperform, in terms of AUC, radiation oncologists using guidelines' recommendation currently used in clinical practice [135].

In particular, the possibility of decreasing toxic treatments in case of minimal improvements as well as boosting the treatment in case of high likelihood of failure/recurrence [78] is a way to pave the road of personalized medicine. Imaging is at present used in oncology for guiding and in some instances for adapting therapies, and most if not all these trials rely on using volumetric information. Clinical trials are needed to further validate the importance and additive role of radiomics in a clinical setting [18].

Radiomics provides a way to reduce costs in health care. First, radiomics is relatively cost-effective given that images are already available for most patients in oncology [88]. Second, radiomics could reduce the need for biopsy, which is invasive nature and has high associated risk and cost [27]. Third, by providing early identification of patients who do not respond to chemotherapy, it has also the advantage of avoiding unnecessary treatment with its risk of toxicity.

Technically, approaches that look into longitudinal variations in radiomic features would be useful such as in delta-radiomics, the analysis of the percentage change of radiomic features assessed in repeated scans during the course of chemo and radiotreatment [136,137]. It has been shown that radiotherapy induces changes in textural features in the tumor during the treatment, which are related to prognosis [107]. Mid treatment information from PET/MR or even daily Cone Beam CT (CBCT) images, currently acquired for alignment setup, could be applied [137] for adapting intensity-modulated radiotherapy in order to boost radioresistant tumors or tumor subvolumes (e.g. hypoxic). Also organs at risk could benefit by radiomics-adapted radiotherapy, as early changes of textural features in some organs during the treatment are related to the appearance of side effects, for example xerostomia [138].

Another approach to study temporal variations is within the acquisition process. Such is the case of dynamic PET or MRI [38], so that, instead of currently used static features, dynamic features inter- and intra-acquisitions could be used.

5.6. Conclusion

Medicine will evolve toward individualized approaches in many fields, driven by the need to increase safety, improve efficacy, decrease the drug development costs as well as shorten time-to-market. New imaging capabilities, e.g. with the development of phase-contrast CT, the introduction of a large number of innovative MRI sequences and the progress of radiotracers in molecular imaging, will fuel the evolution of radiomics to create a minimally invasive, cost-affordable way to the road of personalized medicine.

Appendix: Image preprocessing

A.1. Resampling

Prior to the calculation of radiomic features, it is advised resampling to isotropic voxel size to have standardized voxel spacing across the cohort [15]. For example, CT images with average voxel spacing of $0.9 \times 0.9 \times 3$ mm^3 respectively for (x, y, z) were resampled to $3 \times 3 \times 3$ mm^3 [55].

A.2. Discretization

In discretization, voxel intensities are grouped into equally spaced ranges or "bins" in order to reduce image noise and normalize intensities across all different patients. This process, called quantization or discretization or resampling, also improves efficiency of computation of radiomic features [123]. High discretization levels provide more detail at the cost of increased noise, while resampling at fewer than 32 quantization levels may remove significant texture information from the images [84].The two methods commonly used to discretize are: (1) fixed bin size, or intensity resolution, in units of voxel intensity, such as 25 Hounsfield Units in CT [55] and (2) a fixed number of bins, as 32 or 64, which also determines the size of the matrices for texture analysis [41]. In the work of Leijenaar et al., these two different discretization methods where compared for several textural features extracted from SUV maps in order to identify which is most appropriate in a clinical setting. Textural features, calculated from GLCM, GLRLM, GLSZM, were shown to depend on the intensity resolution used for SUV discretization. It was also shown that maintaining a constant intensity resolution across tumor images yields textural feature values that are defined on the same SUV scale, allowing for a meaningful comparison of texture between images. When fixed bin size in units SUV was used, patient rankings for several

features were affected by the choice of intensity resolution [129]. Some authors have suggested 64 bins as an optimum scheme for providing the highest degree of reproducibility and robustness [139].

A.3. Filtration

Filters can be applied to images to enhance image characteristics such as edges or textures, then features can be extracted from the images obtained without filtration and those obtained with filtration [21]. Spatial filtering techniques are based on the convolution of the input image with the desired kernel to produce filtered images [13]. The filters or kernels of size $n \times n$ determine the size of the neighborhood considered by the kernel. Some examples of commonly used filters for texture analysis include statistical filters like average filter, range filter, and entropy filter. Edge filters, such as Kirsch [140] and Sobel filters [78], result in edge enhancement by calculating an approximation of the derivatives in horizontal and vertical directions. The two gradient approximations can be combined into a gradient magnitude [78].

The Laplacian of an image brings out area of rapid intensity change and is usually used for edge detection. Gaussian bandpass filter smooths the image and reduces noise through convolution with a Gaussian kernel [14,28,56]. These are often used together, resulting in the Laplacian of Gaussian filter which extracts areas with increasingly coarse texture patterns, by tuning the standard deviation of the Gaussian filter [14].

Some kernels have been designed for identifying specific textures of an image. For example, Laws' filters were generated from 5 basic vectors or a combination of them, to emphasize image textures of edge, spot, ripple, wave, undulation and oscillation. Laws texture energy measures have been used in filtering input medical images for texture analysis in radiomics [100].

Wavelet transforms decompose the original image, similarly as Fourier analysis, but in both space and frequency domains. They have been used for image enhancement of microcalcification in CAD for breast cancer, where the ROI is decomposed into its subbands using the wavelet transformation and to the coefficients of the subbands are weighted so that microcalcifications are enhanced. After wavelet inverse transform is applied to the data background tissue and noise are suppressed [7].

A 1-D wavelet transform can be applied iteratively to CT images along all three directions, decomposing the original image into multiple components, which are then interpreted as the result from filtering of the image with a low-pass or high-pass filters along x-, y- and z-direction [89,141]. As an example, a wavelet filtered image called "LHL" is the result of applying low, high and low pass filters on the x, y, z direction respectively.

References

[1] Doi K. Computer-aided diagnosis in medical imaging: historical review, current status and future potential. Comput Med Imaging Graph 2007;31:198–211.
[2] Tang J, Rangayyan RM, Xu J, El Naqa I, Yang Y. Computer-aided detection and diagnosis of breast cancer with mammography: recent advances. IEEE Trans Inf Technol Biomed 2009;13:236–51.
[3] Giger ML, Karssemeijer N, Schnabel JA. Breast image analysis for risk assessment, detection, diagnosis, and treatment of cancer. Annu Rev Biomed Eng 2013;15:327–57.
[4] Summers RM. Texture analysis in radiology: does the emperor have no clothes? Abdom Radiol (NY) 2017;42(2):342–5.
[5] Dhungel N, Carneiro G, Bradley AP. A deep learning approach for the analysis of masses in mammograms with minimal user intervention. Med Image Anal 2017;37:114–28.
[6] El Naqa I, Li R, Murphy MJ, editors. Machine learning in radiation oncology: theory and applications. SpringerLink; 2015.
[7] Elter M, Horsch A. CADx of mammographic masses and clustered microcalcifications: a review. Med Phys 2009;36:2052–68.
[8] Kuo MD, Gollub J, Sirlin CB, Ooi C, Chen X. Radiogenomic analysis to identify imaging phenotypes associated with drug response gene expression programs in hepatocellular carcinoma. J Vasc Interv Radiol 2007;18:821–30.
[9] El Naqa I, Grigsby P, Apte A, Kidd E, Donnelly E, Khullar D, et al. Exploring feature-based approaches in PET images for predicting cancer treatment outcomes. Pattern Recognit 2009;42:1162–71.
[10] Kumar V, Gu Y, Eschrich S, Eikman EA, Berman C, Goldgof D, et al. Radiomics of non small cell lung cancer: association of quantitative image features with histology and outcomes. Mol Imag Biol 2010;12(Suppl 2):S1213.
[11] Gillies RJ, Anderson AR, Gatenby RA, Morse DL. The biology underlying molecular imaging in oncology: from genome to anatome and back again. Clin Radiol 2010;65:517–21.
[12] Falk M, Hausmann M, Lukasova E, Biswas A, Hildenbrand G, Davidkova M, et al. Determining Omics spatiotemporal dimensions using exciting new nanoscopy techniques to assess complex cell responses to DNA damage: part A–radiomics. Crit Rev Eukaryot Gene Expr 2014;24:205–23.
[13] Parekh V, Jacobs MA. Radiomics: a new application from established techniques. Expert Rev Precis Med Drug Dev 2016;1:207–26.
[14] Gillies RJ, Kinahan PE, Hricak H. Radiomics: images are more than pictures, they are data. Radiology 2016;278:563–77.
[15] Vallieres M, Freeman CR, Skamene SR, El Naqa I. A radiomics model from joint FDG-PET and MRI texture features for the prediction of lung metastases in soft-tissue sarcomas of the extremities. Phys Med Biol 2015;60:5471–96.
[16] Aerts HJ, Velazquez ER, Leijenaar RT, Parmar C, Grossmann P, Carvalho S, et al. Decoding tumour phenotype by noninvasive imaging using a quantitative radiomics approach. Nat Commun 2014;5:4006.
[17] Lambin P, Rios-Velazquez E, Leijenaar R, Carvalho S, van Stiphout RG, Granton P, et al. Radiomics: extracting more information from medical images using advanced feature analysis. Eur J Cancer 2012;48:441–6.
[18] Kotrotsou A, Zinn PO, Colen RR. Radiomics in brain tumors: an emerging technique for characterization of tumor environment. Magn Reson Imaging Clin N Am 2016;24:719–29.
[19] Panth KM, Leijenaar RT, Carvalho S, Lieuwes NG, Yaromina A, Dubois L, et al. Is there a causal relationship between genetic changes and radiomics-based image features? An in vivo preclinical experiment with doxycycline inducible GADD34 tumor cells. Radiother Oncol 2015;116:462–6.
[20] Kumar V, Gu Y, Basu S, Berglund A, Eschrich SA, Schabath MB, et al. Radiomics: the process and the challenges. Magn Reson Imaging 2012;30:1234–48.
[21] Huang Y, Liu Z, He L, Chen X, Pan D, Ma Z, et al. Radiomics signature: a potential biomarker for the prediction of disease-free survival in early-stage (I or II) non-small cell lung cancer. Radiology 2016;152234.
[22] Hoffman J, Young S, Noo F, McNitt-Gray M. Technical Note: FreeCT_wFBP: a robust, efficient, open-source implementation of weighted filtered backprojection for helical, fan-beam CT. Med Phys 2016;43:1411–20.
[23] Yu J, Shi Z, Ji C, Lian Y, Wang Y, Chen L, et al. Anatomical location differences between mutated and wild-type isocitrate dehydrogenase 1 in low-grade gliomas. Int J Neurosci 2016. http://dx.doi.org/10.1080/00207454.2016.1270278.
[24] Tagliaferri L, Kovàcs G, Autorino R, Budrukkar A, Guinot JL, Hildebrand G, et al. ENT COBRA (consortium for brachytherapy data analysis): interdisciplinary standardized data collection system for head and neck patients treated with interventional radiotherapy (brachytherapy). J Contemp Brachyther 2016;8:336–43.
[25] Yoon HJ, Sohn I, Cho JH, Lee HY, Kim JH, Choi YL, et al. Decoding tumor phenotypes for ALK, ROS1, and RET fusions in lung adenocarcinoma using a radiomics approach. Medicine (Baltimore) 2015;94:e1753.
[26] Parmar C, Grossmann P, Bussink J, Lambin P, Aerts HJ. Machine learning methods for quantitative radiomic biomarkers. Sci Rep 2015;5:13087.
[27] Parmar C, Leijenaar RTH, Grossmann P, Velazquez ER, Bussink J, Rietveld D, et al. Radiomic feature clusters and prognostic signatures specific for lung and head neck cancer. Sci Rep 2015;5.
[28] Coroller TP, Grossmann P, Hou Y, Rios Velazquez E, Leijenaar RT, Hermann G, et al. CT-based radiomic signature predicts distant metastasis in lung adenocarcinoma. Radiother Oncol 2015;114:345–50.
[29] Giesel F, Schneider F, Kratochwil C, Rath D, Holland-Letz T, Moltz J, et al. CT radiomic analysis using lymph-node-density profile in correlation to SUV-value for PET/CT based N-Staging. J Nucl Med 2016.
[30] McNitt-Gray MF, Hart EM, Wyckoff N, Sayre JW, Goldin JG, Aberle DR. A pattern classification approach to characterizing solitary pulmonary nodules imaged on high resolution CT: preliminary results. Med Phys 1999;26:880–8.
[31] Ganeshan B, Goh V, Mandeville HC, Ng QS, Hoskin PJ, Miles KA. Non-small cell lung cancer: histopathologic correlates for texture parameters at CT. Radiology 2013;266:326–36.
[32] Ganeshan B, Abaleke S, Young RC, Chatwin CR, Miles KA. Texture analysis of non-small cell lung cancer on unenhanced computed tomography: initial evidence for a relationship with tumour glucose metabolism and stage. Cancer Imaging 2010;10:137–43.
[33] Karlo CA, Di Paolo PL, Chaim J, Hakimi AA, Ostrovnaya I, Russo P, et al. Radiogenomics of clear cell renal cell carcinoma: associations between CT imaging features and mutations. Radiology 2014;270:464–71.
[34] Ypsilantis PP, Siddique M, Sohn HM, Davies A, Cook G, Goh V, et al. Predicting response to neoadjuvant chemotherapy with PET imaging using convolutional neural networks. PLoS One 2015;10:e0137036.

[35] Dhingra VK, Mahajan A, Basu S. Emerging clinical applications of PET based molecular imaging in oncology: the promising future potential for evolving personalized cancer care. Indian J Radiol Imaging 2015;25:332–41.
[36] Antunes J, Viswanath S, Rusu M, Valls L, Hoimes C, Avril N, et al. Radiomics analysis on FLT-PET/MRI for characterization of early treatment response in renal cell carcinoma: a proof-of-concept study. Transl Oncol 2016;9:155–62.
[37] Lu L, Lv W, Jiang J, Ma J, Feng Q, Rahmim A. Robustness of radiomic features in [11C]choline and [18F]FDG PET/CT imaging of nasopharyngeal carcinoma: impact of segmentation and discretization. Mol Imaging Biol 2016;18(6):935–45.
[38] Naqa IE. The role of quantitative PET in predicting cancer treatment outcomes. Clin Trans Imaging 2014;2:305–20.
[39] Grigsby PW, Siegel BA, Dehdashti F, Rader J, Zoberi I. Posttherapy [18F] fluorodeoxyglucose positron emission tomography in carcinoma of the cervix: response and outcome. J Clin Oncol 2004;22:2167–71.
[40] Berghmans T, Dusart M, Paesmans M, Hossein-Foucher C, Buvat I, Castaigne C. Primary tumor standardized uptake value (SUVmax) measured on fluorodeoxyglucose positron emission tomography (FDG-PET) is of prognostic value for survival in non-small cell lung cancer (NSCLC): a systematic review and meta-analysis (MA) by the European lung cancer working party for the IASLC lung cancer staging project. J Thorac Oncol 2008;3:6–12.
[41] Hatt M, Tixier F, Pierce L, Kinahan PE, Le Rest CC, Visvikis D. Characterization of PET/CT images using texture analysis: the past, the presentEllipsis any future? Eur J Nucl Med Mol Imaging 2017;44:151–65.
[42] van Stiphout RGPM, Lammering G, Buijsen J, Janssen MHM, Gambacorta MA, Slagmolen P. Development and external validation of a predictive model for pathological complete response of rectal cancer patients including sequential PET-CT imaging. Radiotherapy Oncol 2011;98:126–33.
[43] Ohri N, Duan F, Snyder BS, Wei B, Machtay M, Alavi A, et al. Pretreatment 18F-FDG PET textural features in locally advanced non-small cell lung cancer: secondary analysis of ACRIN 6668/RTOG 0235. J Nucl Med 2016;57:842–8.
[44] Earnest 4th F, Kelly PJ, Scheithauer BW, Kall BA, Cascino TL, Ehman RL, et al. Cerebral astrocytomas: histopathologic correlation of MR and CT contrast enhancement with stereotactic biopsy. Radiology 1988;166:823–7.
[45] Khalvati F, Wong A, Haider MA. Automated prostate cancer detection via comprehensive multi-parametric magnetic resonance imaging texture feature models. BMC Med Imaging 2015;15. 27-015-0069-9.
[46] Cameron A, Khalvati F, Haider MA, Wong A. MAPS: a quantitative radiomics approach for prostate cancer detection. IEEE Trans Biomed Eng 2016;63:1145–56.
[47] Bhooshan N, Giger ML, Jansen SA, Li H, Lan L, Newstead GM. Cancerous breast lesions on dynamic contrast-enhanced MR images: computerized characterization for image-based prognostic markers. Radiology 2010;254:680–90.
[48] Nie K, Shi L, Chen Q, Hu X, Jabbour S, Yue N, et al. Rectal cancer: assessment of neoadjuvant chemo-radiation outcome based on radiomics of multi-parametric MRI. Clin Cancer Res 2016.
[49] Li H, Zhu Y, Burnside ES, Huang E, Drukker K, Hoadley KA, et al. Quantitative MRI radiomics in the prediction of molecular classifications of breast cancer subtypes in the TCGA/TCIA data set. NPJ Breast Cancer 2016;2:16012.
[50] Farber NJ, Wu Y, Zou L, Belani P, Singer EA. Challenges in RCC imaging: renal insufficiency, post-operative surveillance, and the role of radiomics. Kidney Cancer J 2015;13:84–90.
[51] McGarry SD, Hurrell SL, Kaczmarowski AL, Cochran EJ, Connelly J, Rand SD, et al. Magnetic resonance imaging-based radiomic profiles predict patient prognosis in newly diagnosed glioblastoma before therapy. Tomography 2016;2:223–8.
[52] Yang D, Rao G, Martinez J, Veeraraghavan A, Rao A. Evaluation of tumor-derived MRI-texture features for discrimination of molecular subtypes and prediction of 12-month survival status in glioblastoma. Med Phys 2015;42:6725–35.
[53] Kickingereder P, Burth S, Wick A, Gotz M, Eidel O, Schlemmer HP, et al. Radiomic profiling of glioblastoma: identifying an imaging predictor of patient survival with improved performance over established clinical and radiologic risk models. Radiology 2016;280(3):880–9.
[54] Wu W, Parmar C, Grossmann P, Quackenbush J, Lambin P, Bussink J, et al. Exploratory study to identify radiomics classifiers for lung cancer histology. Front Oncol 2016;6:71.
[55] Coroller TP, Agrawal V, Narayan V, Hou Y, Grossmann P, Lee SW, et al. Radiomic phenotype features predict pathological response in non-small cell lung cancer. Radiother Oncol 2016;119(3):480–6.
[56] Huynh E, Coroller TP, Narayan V, Agrawal V, Hou Y, Romano J, et al. CT-based radiomic analysis of stereotactic body radiation therapy patients with lung cancer. Radiother Oncol 2016;120(2):258–66.
[57] Tan Y, Schwartz LH, Zhao B. Segmentation of lung lesions on CT scans using watershed, active contours, and Markov random field. Med Phys 2013;40:043502.
[58] Mattonen SA, Palma DA, Johnson C, Louie AV, Landis M, Rodrigues G, et al. Detection of local cancer recurrence after stereotactic ablative radiation therapy for lung cancer: physician performance versus radiomic assessment. Int J Radiat Oncol Biol Phys 2016;94:1121–8.
[59] Mattonen SA, Tetar S, Palma DA, Louie AV, Senan S, Ward AD. Imaging texture analysis for automated prediction of lung cancer recurrence after stereotactic radiotherapy. J Med Imaging (Bellingham) 2015;2:041010.
[60] Liu Y, Kim J, Balagurunathan Y, Li Q, Garcia AL, Stringfield O, et al. Radiomic features are associated with EGFR mutation status in lung adenocarcinomas. Clin Lung Cancer 2016;17(5):441–8.
[61] Rios Velazquez E, Aerts HJWL, Gu Y, Goldgof DB, De Ruysscher D, Dekker A, et al. A semiautomatic CT-based ensemble segmentation of lung tumors: comparison with oncologists' delineations and with the surgical specimen. Radiother Oncol 2012;105:167–73.
[62] Oliver JA, Budzevich M, Zhang GG, Dilling TJ, Latifi K, Moros EG. Variability of image features computed from conventional and respiratory-gated PET/CT images of lung cancer. Transl Oncol 2015;8:524–34.
[63] Lian C, Ruan S, Denoeux T, Jardin F, Vera P. Selecting radiomic features from FDG-PET images for cancer treatment outcome prediction. Med Image Anal 2016;32:257–68.
[64] Zaidi H, El Naqa I. PET-guided delineation of radiation therapy treatment volumes: a survey of image segmentation techniques. Eur J Nucl Med Mol Imaging 2010;37:2165–87.
[65] Van Rossum PSN, Fried DV, Zhang L, Hofstetter WL, Van Vulpen M, Meijer GJ, et al. The incremental value of subjective and quantitative assessment of 18F-FDG PET for the prediction of pathologic complete response to preoperative chemoradiotherapy in esophageal cancer. J Nucl Med 2016;57:691–700.
[66] Li H, Zhu Y, Burnside ES, Drukker K, Hoadley KA, Fan C, et al. MR imaging radiomics signatures for predicting the risk of breast cancer recurrence as given by research versions of mammaPrint, Oncotype DX, and PAM50 gene assays. Radiology 2016;281(2):382–91.
[67] Chen W, Giger ML, Bick U. A fuzzy c-means (FCM)-based approach for computerized segmentation of breast lesions in dynamic contrast-enhanced MR images. Acad Radiol 2006;13:63–72.
[68] Wang J, Kato F, Oyama-Manabe N, Li R, Cui Y, Tha KK, et al. Identifying triple-negative breast cancer using background parenchymal enhancement heterogeneity on dynamic contrast-enhanced MRI: a pilot radiomics study. PLoS One 2015;10:e0143308.
[69] Klifa C, Carballido-Gamio J, Wilmes L, Laprie A, Lobo C, Demicco E. Quantification of breast tissue index from MR data using fuzzy clustering. Conf Proc IEEE Eng Med Biol Soc 2004;3:1667–70.
[70] Echegaray S, Gevaert O, Shah R, Kamaya A, Louie J, Kothary N, et al. Core samples for radiomics features that are insensitive to tumor segmentation: method and pilot study using CT images of hepatocellular carcinoma. J Med Imaging (Bellingham) 2015;2:041011.
[71] Porz N, Bauer S, Pica A, Schucht P, Beck J, Verma RK, et al. Multi-modal glioblastoma segmentation: man versus machine. PLoS One 2014;9:e96873.
[72] Zhang L, Fried DV, Fave XJ, Hunter LA, Yang J, Court LE. IBEX: an open infrastructure software platform to facilitate collaborative work in radiomics. Med Phys 2015;42:1341–53.
[73] Fang Y-D, Lin C-, Shih M-, Wang H-, Ho T-, Liao C-, et al. Development and evaluation of an open-source software package "cGITA" for quantifying tumor heterogeneity with molecular images. BioMed Res Int 2014;2014:248505. http://dx.doi.org/10.1155/2014/248505.
[74] Szczypinski PM, Strzelecki M, Materka Andrzej, Materka A, Klepaczko Artur, Klepaczko A. MaZda – a software package for image texture analysis. Comput Methods Programs Biomed 2009;94(1):66–76.
[75] Chen W, Giger ML, Lan L, Bick U. Computerized interpretation of breast MRI: investigation of enhancement-variance dynamics. Med Phys 2004;31:1076–82.
[76] Guo W, Li H, Zhu Y, Lan L, Yang S, Drukker K, et al. Prediction of clinical phenotypes in invasive breast carcinomas from the integration of radiomics and genomics data. J Med Imaging (Bellingham) 2015;2:041007.
[77] Haralick RM, Shanmugam K, Dinstein I. Textural features for image classification. IEEE Trans Syst Man Cybern 1973;3:610–21.
[78] Gnep K, Fargeas A, Gutierrez-Carvajal RE, Commandeur F, Mathieu R, Ospina JD, et al. Haralick textural features on T2 -weighted MRI are associated with biochemical recurrence following radiotherapy for peripheral zone prostate cancer. J Magn Reson Imaging 2017;45(1):103–17.
[79] Tixier F, Hatt M, Valla C, Fleury V, Lamour C, Ezzouhri S, et al. Visual versus quantitative assessment of intratumor 18F-FDG PET uptake heterogeneity: prognostic value in non-small cell lung cancer. J Nucl Med 2014;55:1235–41.
[80] Chicklore S, Goh V, Siddique M, Roy A, Marsden PK, Cook GJ. Quantifying tumour heterogeneity in 18F-FDG PET/CT imaging by texture analysis. Eur J Nucl Med Mol Imaging 2013;40:133–40.
[81] Galloway MM. Texture analysis using gray level run lengths. Comp Graphics Image Process 1975;4:172–9.
[82] Tixier F, Le Rest CC, Hatt M, Albarghach N, Pradier O, Metges JP, et al. Intratumor heterogeneity characterized by textural features on baseline 18F-FDG PET images predicts response to concomitant radiochemotherapy in esophageal cancer. J Nucl Med 2011;52:369–78.
[83] Amadasun M, King R. Textural features corresponding to textural properties. IEEE Trans Syst Man Cybern 1989;19:1264–74.
[84] Bashir U, Siddique MM, Mclean E, Goh V, Cook GJ. Imaging heterogeneity in lung cancer: techniques, applications, and challenges. AJR Am J Roentgenol 2016;207:534–43.
[85] Rangayyan RM, Nguyen TM. Fractal analysis of contours of breast masses in mammograms. J Digit Imaging 2007;20:223–37.
[86] Szigeti K, Szabo T, Korom C, Czibak I, Horvath I, Veres DS, et al. Radiomics-based differentiation of lung disease models generated by polluted air based on X-ray computed tomography data. BMC Med Imaging 2016;16. 14-016-0118-z.

[87] van Velden FH, Kramer GM, Frings V, Nissen IA, Mulder ER, de Langen AJ, et al. Repeatability of radiomic features in non-small-cell lung cancer [18F]FDG-PET/CT studies: impact of reconstruction and delineation. Mol Imaging Biol 2016;18(5):788–95.
[88] Parmar C, Grossmann P, Rietveld D, Rietbergen MM, Lambin P, Aerts HJ. Radiomic machine-learning classifiers for prognostic biomarkers of head and neck cancer. Front Oncol 2015;5:272.
[89] Kickingereder P, Gotz M, Muschelli J, Wick A, Neuberger U, Shinohara RT, et al. Large-scale radiomic profiling of recurrent glioblastoma identifies an imaging predictor for stratifying anti-angiogenic treatment response. Clin Cancer Res 2016;22(23):5765–71.
[90] Huang YQ, Liang CH, He L, Tian J, Liang CS, Chen X, et al. Development and validation of a radiomics nomogram for preoperative prediction of lymph node metastasis in colorectal cancer. J Clin Oncol 2016;34:2157–64.
[91] Liang C, Huang Y, He L, Chen X, Ma Z, Dong D, et al. The development and validation of a CT-based radiomics signature for the preoperative discrimination of stage I-II and stage III-IV colorectal cancer. Oncotarget 2016;7(21):31401–12.
[92] Chen Y, Liu MZ, Liang SB, Zong JF, Mao YP, Tang LL, et al. Preliminary results of a prospective randomized trial comparing concurrent chemoradiotherapy plus adjuvant chemotherapy with radiotherapy alone in patients with locoregionally advanced nasopharyngeal carcinoma in endemic regions of china. Int J Radiat Oncol Biol Phys 2008;71:1356–64.
[93] Chen S, Zhou S, Yin FF, Marks LB, Das SK. Investigation of the support vector machine algorithm to predict lung radiation-induced pneumonitis. Med Phys 2007;34:3808–14.
[94] Wang X, Markowetz F, De Sousa E, Melo F, Medema JP, Vermeulen L. Dissecting cancer heterogeneity–an unsupervised classification approach. Int J Biochem Cell Biol 2013;45:2574–9.
[95] Avanzo M, Trovo M, Furlan C, Barresi L, Linda A, Stancanello J, et al. Normal tissue complication probability models for severe acute radiological lung injury after radiotherapy for lung cancer. Phys Med 2015;31:1–8.
[96] Zhu Y, Li H, Guo W, Drukker K, Lan L, Giger ML, et al. Deciphering genomic underpinnings of quantitative MRI-based radiomic phenotypes of invasive breast carcinoma. Sci Rep 2015;5:17787.
[97] Coroller TP, Agrawal V, Huynh E, Narayan V, Lee SW, Mak RH, et al. Radiomic-based pathological response prediction from primary tumors and lymph nodes in NSCLC. J Thorac Oncol 2017;12(3):467–76.
[98] Ahmed A, Gibbs P, Pickles M, Turnbull L. Texture analysis in assessment and prediction of chemotherapy response in breast cancer. J Magn Reson Imaging 2013;38:89–101.
[99] Liu J, Mao Y, Li Z, Zhang D, Zhang Z, Hao S, et al. Use of texture analysis based on contrast-enhanced MRI to predict treatment response to chemoradiotherapy in nasopharyngeal carcinoma. J Magn Reson Imaging 2016;44:445–55.
[100] Aerts HJ, Grossmann P, Tan Y, Oxnard GG, Rizvi N, Schwartz LH, et al. Defining a radiomic response phenotype: a pilot study using targeted therapy in NSCLC. Sci Rep 2016;6:33860.
[101] Fried DV, Mawlawi O, Zhang L, Fave X, Zhou S, Ibbott G, et al. Stage III non-small cell lung cancer: prognostic value of FDG PET quantitative imaging features combined with clinical prognostic factors. Radiology 2016;278:214–22.
[102] Diehn M, Nardini C, Wang DS, McGovern S, Jayaraman M, Liang Y, et al. Identification of noninvasive imaging surrogates for brain tumor gene-expression modules. Proc Natl Acad Sci USA 2007;105:5213–8.
[103] Lee J, Narang S, Martinez JJ, Rao G, Rao A. Associating spatial diversity features of radiologically defined tumor habitats with epidermal growth factor receptor driver status and 12-month survival in glioblastoma: methods and preliminary investigation. J Med Imaging (Bellingham) 2015;2:041006.
[104] Prasanna P, Patel J, Partovi S, Madabhushi A, Tiwari P. Radiomic features from the peritumoral brain parenchyma on treatment-naive multi-parametric MR imaging predict long versus short-term survival in glioblastoma multiforme: preliminary findings. Eur Radiol 2016.
[105] Permuth JB, Choi J, Balarunathan Y, Kim J, Chen DT, Chen L, et al. Combining radiomic features with a miRNA classifier may improve prediction of malignant pathology for pancreatic intraductal papillary mucinous neoplasms. Oncotarget 2016. http://dx.doi.org/10.1007/s00330-016-4637-3.
[106] Harrison LC, Luukkaala T, Pertovaara H, Saarinen TO, Heinonen TT, Jarvenpaa R, et al. Non-Hodgkin lymphoma response evaluation with MRI texture classification. J Exp Clin Cancer Res 2009;28. 87-9966-28-87.
[107] Cunliffe A, Armato 3rd SG, Castillo R, Pham N, Guerrero T, Al-Hallaq HA. Lung texture in serial thoracic computed tomography scans: correlation of radiomics-based features with radiation therapy dose and radiation pneumonitis development. Int J Radiat Oncol Biol Phys 2015;91:1048–56.
[108] Zhang J, Yu C, Jiang G, Liu W, Tong L. 3D texture analysis on MRI images of Alzheimer' disease. Brain Imaging and Behavior 2012;6:61–9.
[109] Sikio M, Holli-Helenius KK, Harrison LC, Ryymin P, Ruottinen H, Saunamaki T, et al. MR image texture in Parkinson's disease: a longitudinal study. Acta Radiol 2015;56(1):97–104.
[110] Zhang J, Tong L, Wang L, Li N. Texture analysis of multiple sclerosis: a comparative study. Magn Reson Imaging 2008;26:1160–6.
[111] Garcia G, Maiora J, Tapia A, De Blas M. Evaluation of texture for classification of abdominal aortic aneurysm after endovascular repair. J Digit Imaging 2012;25:369–76.
[112] Kotze CW, Rudd JH, Ganeshan B, Menezes LJ, Brookes J, Agu O, et al. CT signal heterogeneity of abdominal aortic aneurysm as a possible predictive biomarker for expansion. Atherosclerosis 2014;233:510–7.
[113] Leijenaar RT, Carvalho S, Velazquez ER, van Elmpt WJ, Parmar C, Hoekstra OS, et al. Stability of FDG-PET Radiomics features: an integrated analysis of test-retest and inter-observer variability. Acta Oncol 2013;52:1391–7.
[114] Mackin D, Fave X, Zhang L, Fried D, Yang J, Taylor B, et al. Measuring computed tomography scanner variability of radiomics features. Invest Radiol 2015;50:757–65.
[115] Kim H, Park CM, Lee M, Park SJ, Song YS, Lee JH, et al. Impact of reconstruction algorithms on CT radiomic features of pulmonary tumors: analysis of intra- and inter-reader variability and inter-reconstruction algorithm variability. PLoS One 2016;11:e0164924.
[116] Zhao B, Tan Y, Tsai WY, Qi J, Xie C, Lu L, et al. Reproducibility of radiomics for deciphering tumor phenotype with imaging. Sci Rep 2016;6:23428.
[117] Zhao B, James LP, Moskowitz CS, Guo P, Ginsberg MS, Lefkowitz RA, et al. Evaluating variability in tumor measurements from same-day repeat CT scans of patients with non-small cell lung cancer. Radiology 2009;252:263–72.
[118] Desseroit MC, Tixier F, Weber WA, Siegel BA, Cheze Le Rest C, Visvikis D, et al. Reliability of PET/CT shape and heterogeneity features in functional and morphological components of non-small cell lung cancer tumors: a repeatability analysis in a prospective multi-center cohort. J Nucl Med 2017;58(3):406–11.
[119] Galavis PE, Hollensen C, Jallow N, Paliwal B, Jeraj R. Variability of textural features in FDG PET images due to different acquisition modes and reconstruction parameters. Acta Oncol 2010;49:1012–6.
[120] Leijenaar RT, Carvalho S, Hoebers FJ, Aerts HJ, van Elmpt WJ, Huang SH, et al. External validation of a prognostic CT-based radiomic signature in oropharyngeal squamous cell carcinoma. Acta Oncol 2015;54:1423–9.
[121] Bailly C, Bodet-Milin C, Couespel S, Necib H, Kraeber-Bodéré F, Ansquer C, et al. Revisiting the robustness of PET-based textural features in the context of multi-centric trials. PLoS One 2016;11(7):e0159984.
[122] Grootjans W, Tixier F, van der Vos CS, Vriens D, Le Rest CC, Bussink J, et al. The impact of optimal respiratory gating and image noise on evaluation of intra-tumor heterogeneity in 18F-FDG positron emission tomography imaging of lung cancer. J Nucl Med 2016;17(5). 441–448.e6.
[123] Yip SS, Aerts HJ. Applications and limitations of radiomics. Phys Med Biol 2016;61:R150–66.
[124] Parmar C, Rios Velazquez E, Leijenaar R, Jermoumi M, Carvalho S, Mak RH, et al. Robust Radiomics feature quantification using semiautomatic volumetric segmentation. PLoS One 2014;9:e102107.
[125] Napel S, Giger M. Special section guest editorial: radiomics and imaging genomics: quantitative imaging for precision medicine. J Med Imaging (Bellingham) 2015;2:041001.
[126] Sala E, Mema E, Himoto Y, Veeraraghavan H, Brenton JD, Snyder A, et al. Unravelling tumour heterogeneity using next-generation imaging: radiomics, radiogenomics, and habitat imaging. Clin Radiol 2017;72:3–10.
[127] Li H, Zhu Y, Burnside ES, Drukker K, Hoadley KA, Fan C, et al. MR imaging radiomics signatures for predicting the risk of breast cancer recurrence as given by research versions of MammaPrint, Oncotype DX, and PAM50 gene assays. Radiology 2016;281:382–91.
[128] Hatt M, Majdoub M, ValliÃres M, Tixier F, Le Rest CC, Groheux D, et al. 18F-FDG PET uptake characterization through texture analysis: investigating the complementary nature of heterogeneity and functional tumor volume in a multi-cancer site patient cohort. J Nucl Med 2015;56:38–44.
[129] Leijenaar RT, Nalbantov G, Carvalho S, van Elmpt WJ, Troost EG, Boellaard R, et al. The effect of SUV discretization in quantitative FDG-PET Radiomics: the need for standardized methodology in tumor texture analysis. Sci Rep 2015;5:11075.
[130] Radiomics Digital Phantom. Available at: <https://www.cancerdata.org/resource/doi:10.17195/candat.2016.08.1> [accessed 03/20, 2017].
[131] Larue RT, Defraene G, De Ruysscher D, Lambin P, van Elmpt W. Quantitative radiomics studies for tissue characterization: a review of technology and methodological procedures. Br J Radiol 2017;90:20160665.
[132] El Naqa I. Biomedical informatics and panomics for evidence-based radiation therapy. Wiley Interdiscip Rev Data Mining Knowledge Discov 2014;4:327–40.
[133] LeCun Y, Bengio Y, Hinton G. Deep learning. Nature 2015;521:436–44.
[134] Suzuki K. Pixel-based machine learning in medical imaging. Int J Biomed Imaging 2012;2012:792079.
[135] Oberije C, Nalbantov G, Dekker A, Boersma L, Borger J, Reymen B, et al. A prospective study comparing the predictions of doctors versus models for treatment outcome of lung cancer patients: a step toward individualized care and shared decision making. Radiother Oncol 2014;112:37–43.
[136] Carvalho S, Leijenaar RTH, Troost EGC, van Elmpt W, Muratet J, Denis F. Early variation of FDG-PET radiomics features in NSCLC is related to overall survival – the "delta radiomics" concept. Radiother Oncol 2016;118:S20–1.
[137] van Timmeren JE, Leijenaar RTH, van Elmpt W, Lambin P. Can we replace high quality simulation CT by simple kVcone-beam CT images to extract an externally validated radiomics signature? Radiother Oncol 2016;118:S107.
[138] Belli ML, Scalco E, Sanguineti G, Fiorino C, Broggi S, Dinapoli N, et al. Early changes of parotid density and volume predict modifications at the end of therapy and intensity of acute xerostomia. Strahlenther Onkol 2014;190:1001–7.

[139] Tixier F, Hatt M, Le Rest CC, Le Pogam A, Corcos L, Visvikis D. Reproducibility of tumor uptake heterogeneity characterization through textural feature analysis in 18F-FDG PET. J Nucl Med 2012;53:693–700.
[140] Kirsch RA. Computer determination of the constituent structure of biological images. Comput Biomed Res 1971;4:315–28.
[141] Basu B, Basu S. Correlating and combining genomic and proteomic assessment with in vivo molecular functional imaging: will this be the future roadmap for personalized cancer management? Cancer Biother Radiopharm 2016;31:75–84.
[142] Emaminejad N, Qian W, Guan Y, Tan M, Qiu Y, Liu H, et al. Fusion of quantitative image and genomic biomarkers to improve prognosis assessment of early stage lung cancer patients. IEEE Trans Biomed Eng 2016;63:1034–43.
[143] Ghosh P, Tamboli P, Vikram R, Rao A. Imaging-genomic pipeline for identifying gene mutations using three-dimensional intra-tumor heterogeneity features. J Med Imaging (Bellingham) 2015;2:041009.